6-1997

Comparison of outgassing and surface reactivity of graphic substrates

Philip Ross Tavernier
Union College - Schenectady, NY

COMPARISON OF OUTGASSING AND SURFACE REACTIVITY OF GRAPHITIC SUBSTRATES

By

Philip Ross Tavernier

****

Submitted in partial fulfillment

of the requirements for

Honors in the Department of Chemistry

UNION COLLEGE

June, 1997

Dedicated to

Mom and Dad

Preface

The work presented here is a culmination of ten months of research and investigation during my senior year at Union College. Nearly all of the work presented was done at the General Electric Company Corporate Research and Development lab in Niskayuna New York. Funding for this work was provided by the General Electric Corporation. Many thanks go to Professor Karen Lou who served as advisor to this research and provided tremendous encouragement to leave no questions unanswered. I would also like to take this opportunity to recognize the scientists at General Electric who provided input to help me solve all of the problems associated with such research work. Particularly, Tom Raber, Don Lipkin and Dennis Dalpe have earned my highest praise and thanks.

PRT

6/97

Note to Readers: The figures and diagrams have originally been printed in color which improves their readability. If this copy does not contain color plots and figures, the original bound copy in the Union College Chemistry Department may be viewed by any persons wishing to do so. Inquires should be directed to the secretary of the department.

ABSTRACT

TAVERNIER, PHILIP R. Comparison of outgassing and surface reactivity of graphitic substrates. Department of Chemistry, June 1997.

Materials constructed of carbon are widely used in applications requiring high emissivity at temperatures above 1300°C. The ability to transmit heat efficiently makes these materials an excellent choice for use with x-ray tubes. However, heating carbon substrates to high temperatures also leads to thermal desorption of surface bound species. The release of these species increases the total vapor pressure inside sealed x-ray tubes.

Our present study considers the outgassing of these carbon substrates as a function of temperature, as a result of their reactivity towards oxygen, carbon monoxide, carbon dioxide, and water vapor. By modeling the factors that influence outgassing performance in vacuum environments, we can account for and minimize thermal desorption during an x-ray tube's operation.

Work completed to date has uncovered a significant source of outgassing from the surface of the graphite at temperatures approaching 1600°C. The release of carbon monoxide, which occurs readily at these elevated temperatures, corresponds to a binding energy of 450-500 kJ/mol. To explain the desorption of the more strongly bonded molecules, we propose the existence of a carbon-oxygen-carbon bridge between two basal planes of graphite, which had been previously modeled, but not directly observed. Using the results from our own modeling studies, we can suggest a mechanism for this desorption and predict the binding energies associated with the carbon-oxygen-carbon structure. Understanding of the high temperature reaction of carbon will ultimately lead to better materials processing during the manufacturing of x-ray tubes.

Table of Contents

I. Introduction 1

Figures 1.1-1.2 11-12

iI. Experimental 13

A. Vacuum System 14

B. Temperature Control and Measurement 15

C. Dosing Gas Introduction 18

D. *In Situ* Processing Analysis 19

Table 2.1 22

Figures 2.1-2.4 23-25

III. Results 26

Tables 3.1-3.2 42-43

Figures 3.1-3.36 44-62

IV. Discussion 63

Table 4.1 75

Figures 4.1-4.2 76-77

V. Summary 78

VI. Appendices 80

References 81

I. Introduction

The production of carbon monoxide via the gasification of carbon, may be the most important reaction ever studied. Consequently, a tremendous amount of research has been directed toward identifying the principles of materials chemistry involved and understanding all aspects of the reaction. While elucidating the mechanism of this reaction, as well as the kinetic and thermodynamic factors which govern it, has proved difficult, recent studies have made very good progress towards understanding the reaction of carbon at low temperatures. Very little work has been done on the same reaction at temperatures in excess of 1200°C. Our study is thus driven by an attempt to understand the reactivity of carbon at these higher temperatures.

Carbon is generally thought of as the backbone of biological chemistry, but many of its most important uses are in materials chemistry and engineering. A few parts per million of carbon turns iron into high strength steel. Graphite furnaces have been constructed which hold molten metals during treatment. Another important use of carbon is for control rods in nuclear reactors. In fact, much of the materials research on graphite focuses on this use. Carbon also exhibits a very good ability to radiate heat, also known as emissivity. Substances that radiate heat absorb it equally well; this is the property which makes carbon a popular choice for use in x-ray tube substrates. Since x-ray tube targets furnish much of the impetus for this study, it is appropriate to comment in more detail on their requirements as they concern graphite.

The basic construction of an x-ray tube consists of a rotating cathode (substrate) and a stationary anode. The anode, or emitter, is generally a high

resistivity wire that literally blows electrons off its surface which are then accelerated into the cathode. At the surface of the cathode, the electrons collide with atoms knocking inner shell electrons out of their orbits. X-rays are produced after outershell electrons fall towards the nucleus. To maximize the number of x-rays produced, the entire process must occur in a vacuum to limit the number of stray molecules that can interfere with electrons or x-rays. The vacuum requirements vary, but in general, pressures less than a tenth of a millitorr are desirable.

The process of generating electrons and accelerating them onto a rotating cathode surface generates more than just x-rays, it also produces a great deal of thermal energy, which must somehow be dissipated in a non-destructive manner. Some studies estimate the surface temperature of the metal cathode to reach peak temperatures in excess of 1600°C for short periods. Unless this energy is safely channeled away from the source, destruction of the inner workings of the tube could result. (Keep in mind that this entire substrate is also spinning rapidly at about 1000 rpm.) If carbon were bonded to the metal x-ray track, it could be used as a heat sink for the metal surface. Another advantage gained by using graphite is that it is much lighter and less dense than similar metallic substrates. Thus rotating the cathode at higher speeds becomes less of a concern.

Graphite which is bonded to the metal track of the x-ray tube target then has the task of removing this thermal energy in a nondestructive and nontransformative manner. This means that little or no changes in the internal structure of graphite should result, such as recrystallization, phase transformation, or grain growth. The

same studies that estimate such high temperatures for the metal track, also predict that transferred thermal energy may raise the temperature of the graphite to 1200°C for longer time periods. (1) New x-ray tubes may be expected to operate under higher power with less cool-down time, which will push these temperatures maxima even higher.

The high temperatures produced during short x-ray generation are more than sufficient to cause thermal desorption of surface bound species from surfaces within the tube. Research conducted here focuses only on the desorption of species from the graphite surface, but it should be stressed that every exposed element contributes to outgassing and therefore tube pressure. Previous work has established that the hottest and largest part of the x-ray tube, the anode, is responsible for most of the outgassing. In accordance with these findings, we will focus our attention on this one aspect of tube design and processing.

Let us now consider the reactions that carbon, and particularly graphite, undergo which make it interesting to both chemists and material scientists. Oxygen is the most important of several gases that is capable of gasifying carbon according to the following reaction, $2C(s) + O_2(g) \rightarrow 2CO(g)$. Consider the implications of such a reaction; it is possible to gasify a starting solid by exposure to air at room temperature. This will then lead to the release of surface bound carbon-oxygen species during subsequent heating of the material. Many substances undergo similar oxidation reactions with O_2, but the reactions products do not include a volatile gas, as is the case with carbon. Additional reactions at the surface of the graphite can

produce other species; for example, the readsorption of carbon monoxide could lead to the desorption of carbon dioxide. (2) The mechanisms that allow for gasification are quite interesting and will be the subject of some further review.

A complete discussion of the structure of graphite (figure 1.1) can be found in *Solid State Chemistry* by Lesley Smart and Elaine Moore, who calculate the bonding distance between members of the carbon rings to be 1.42 Å, while the spacing between sheets of the rings is 3.35 Å. Without involving ourselves too much in a complete study of the structure, we know that the sheets themselves are held together by weak van der Waals forces while the ring bonding relies on stronger σ bonds. The overlapping $2p$ orbitals form additional π bonds. This tendency to delocalize bonding, in principle, could cause the graphite structure to become much more forgiving to defects within its lattice structure. A missing atom in the plane of the graphite will have a much smaller dislocation energy than a similar defective carbon atom out of the diamond structure. Rearrangements which contort the graphite layers and make them non-planar can be tolerated due to the soft van der Waals forces holding the planes together. Rearrangements in diamonds must break covalent bonds which are much less forgiving when compared with electrostatic attractions. Metals often show the same type of defective structures which can be attributed to the "sea of electron" bonding rather than strict covalent bonding. In graphite these defects take the form of four or five membered rings which are then inserted into the crystal lattice structure, or along surface edges. (3) Figure 1.2c shows a typical surface defect which has resulted in a distorted five membered ring on surface of a single

graphite layer. The reaction of this defect is thought to be intimately involved with the chemisorption of CO onto the surface.

The proposed mechanism of gasification predicts that during chemisorption, molecular oxygen approaches the graphite surface and bonds to the vertices of two six membered rings as shown in figure 1.2a. (4) A bond is formed between C1 and O1 which must result in the breaking of the double bond between O1 and O2. The remaining single bond between these oxygens is severed and the C1 to O1 bond becomes approximately equivalent to a double bond, shown in figure 1.2b. This new species is referred to as a semiquinione group, which may now undergo further reaction in two distinct pathways. (4) Pathway number one is simple desorption of the CO species which results when the C2-C1-C3 bond is broken. The five member ring defect shown in figure 1.2c is left on the graphite surface. Further exposure of this site can, in principle, reform the semiquinione structure at this site. A second reaction pathway can result if an additional molecule of CO is exposed to the semiquinione group. (4) Such a double exposure is plausible if one assumes CO from neighboring sites can be readsorbed. The second intermediate is formed according to figure 1.2d. This species, termed a lactone, can then react to release CO_2, leaving behind the original defect free graphite edge. (4) A combination of both reactions occurring simultaneously explains the desorption of CO and CO_2 from a carbon surface.

The adsorption and release of CO obviously requires the exchange of energy, which will first be discussed qualitatively. A simple view of the surface allows us to reason that if providing an energy of E will break the bonds necessary to release CO,

we will then observe a peak desorption of CO as we approach a temperature providing E kJ/mol. As we shall see, this energy E is actually an activation energy. Once we have defined a temperature or a range of temperatures, we may then work backwards using the Boltzmann expression to find the energy being supplied at these temperatures. This qualitative view works well to develop a basic understanding of the process involved, but breaks down under increased complexity. What follows is a more mathematical approach to desorption of gases first published by P.A. Redhead in 1962. (5)

The best way to investigate the energy of desorbing surface species is to vary the sample's temperature with respect to time. This can be represented by either a linear change ($T = T_o + \beta t$, where β is the change in K per second), or a nonlinear change (ex. $1/T = 1/T_o - \alpha t$, where α is the change per time degree). (5) Additionally, N(t) is some function which described the desorption rate per unit area as a function of time with units of molecules/cm^2/sec. Applying the differential form of the expression, one obtains $-d\sigma/dt = N(t)$. This can also be written as $-d\sigma/dt = A\,\sigma \exp(-E_{des}/RT)$ for a first order desorption reaction, where T is a dependent variable of time. (5) E_{des} is the activation energy of desorption, A is the rate constant (also referred to as the frequency factor) for the first order desorption reaction, and σ is the surface coverage per unit area initially. The exponential term arises from the Arrhenius-like dependence on temperature. Solving N(t) to find the temperature of maximum desorption, T_p, results in the following equation for a first order desorption reaction; (5)

$$E_{des}/RT_p^2 = (A/\beta)\exp(-E_{des}/RT_p) \qquad (1.1)$$

The energy of desorption cannot be solved for directly; instead successive approximations must be carried out to find suitable values for a given T_p and β, by first assuming a value of A. Of course A may be found independently if one does not wish to use an assumed value, by changing β and then plotting the change in T_p as a function of β. (5) In general this exercise usually verifies that $A \approx 10^{13}$ Hz, and our original assumption is good. Of course relationship (1) relies on several simplifying approximations, the most important of which is our characterization that the reaction is indeed first order. A second order equation can be written, but the T_p becomes complicated by a dependence on the initial surface coverage of the desorbing species. (Notice that in eqn 1.1, σ did not appear.) Another assumption we have made is that desorbed molecules do not readsorb back onto the surface of the graphite to any significant extent. This will be supported later by experimental evidence that CO_2, which can form when CO is readsorbed into a semiquinone group, comprises less than 10% of the overall signal. With the appropriate mathematical model now in place, we may quantify the transfer of energy during chemisorption.

An alternative approach to energy considerations arises from a more basic look at the bonds that must be formed or broken during the process. Using a table of average bond energies found in any general chemistry text, we can estimate the average energy required to release CO from a semiquinone type structure found in figure 1.2b. To advance from figure 1.2b to 1.2d, two carbon-carbon bonds of average energy 347 kJ/mol must be broken in order to release one molecule of CO.

(6) A new carbon-carbon bond is formed in turn which releases 347 kJ/mol resulting in a net energy of +347 kJ/mol required for CO removal. This value, which we shall call ΔH, is a better representation of the total change in energy between initial and final states. Estimating the heat of reaction helps us judge the credibility of the reaction mechanism. From the table, a carbon-oxygen double bond has an average energy of 728 kJ/mol, while the carbon-carbon single bond is only 347 kJ/mol. Since breaking two of these carbon-carbon bonds require less energy than breaking one carbon-oxygen double bond, this may help explain why the CO is desorbed rather than molecular oxygen. Obviously we have taken some substantial simplifying assumptions here, but computer aided modeling can be invoked which gives a better estimation of the ΔH_{rxn} and relies more on the quantum mechanical interpretation of bonding.

Computer assisted modeling can provide significant insight into theories describing chemical reactions, but the physical experimentation must be used in order to tie results to physical quantities, such as activation energies. As mentioned earlier, probing the desorption of a species as a function of temperature in an ultrahigh vacuum is an excellent way to establish its bonding energy. This technique is commonly referred to as temperature program desorption, or TPD. Chapter two explains this technique in detail. Additionally, x-ray powder diffraction is useful to establish the crystal structure of the material in question, and to measure the change of the unit cell dimensions with the adsorption of gas. Microscopy, both optical and scanning electron, provides structural information to correlate physical features with

chemisorption reactivity. Spectroscopy of the surface can also provide very valuable information of the chemisorption reactions. Raman, Auger electron, and x-ray photoelectron spectroscopy all contribute to understanding of the exact nature of surface bound species, but were not used during this wcrk due to the unsuitability of our material's microstructure for such studies.

In summary, the nature of the high temperature reaction of graphite has not been very well studied to date, but plausible mechanisms do exist for lower temperature CO desorption. Findings from work focused on the 1000-1200°C range has led to the expectation that significant amounts of CO can be desorbed from carbon above 1200°C. (7) Intercalation of oxygen between basal planes of the graphite has been invoked as a possible explanation for this experimental observation. The goal of our research is to further investigate this high temperature desorption peak and to correlate our results to computerized modeling of the graphite surface. This research will also consider other composite forms of graphite. Since the behavior of these materials is completely unknown, we will study their reactivities at lower temperatures and make comparisons to our standard graphite. Reactivity differences may suggest previously undiscovered surface species which we will also attempt to model. This work should serve to further develop our understanding of carbon materials in order to improve the processing and quality of x-ray tubes.

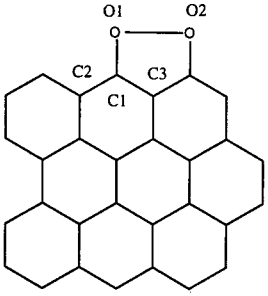

Figure 1.2a

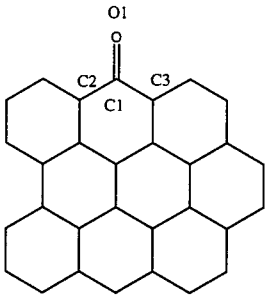

Figure 1.2b

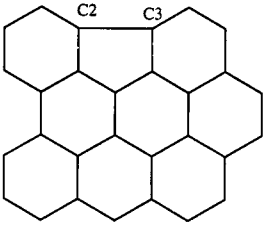

Figure 1.2c

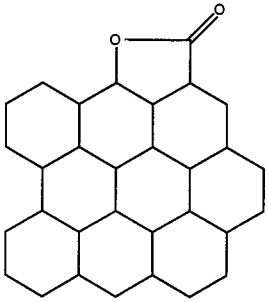

Figure 1.2d

Figure 1.2: Figures a-d show the modeled surface of graphite and the mechanism for chemisorption of oxygen and subsequent desorption of carbon monoxide. Refer to the text for more detail.

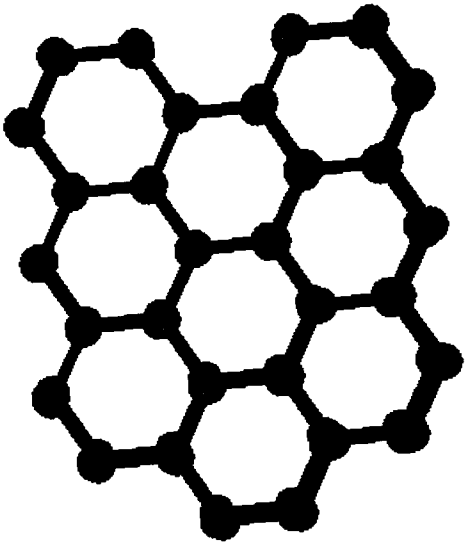

Figure 1.1: Top view of graphite

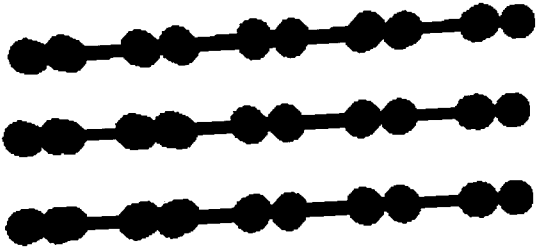

Figure 1.1: Side view of graphite

II. Experimental

In order to conduct useful temperature program desorption, or TPD, experiments, careful control over all aspects of the instrumentation must be maintained. Our system can be broken down in these four areas: the vacuum system, temperature control and measureme· .ng gas introduction, and *in situ* processing analysis. Figure 2.1 shows how each area is assembled into a TPD apparatus.

A. Vacuum System

All samples are dynamically pumped during thermal desorption using a Physical Electronics Ion Pump controlled by a Perkin Elmer power source. The main ion pump chamber consists of a 38 cm diameter stainless steel bell jar connected to the sample chamber via 2 1/2" 304 stainless steel UHV piping. Gate values are placed into this pumping line to allow the sample chamber to be isolated during atmospheric pressurization or gas dosing experiments. Also connected to the sample chamber is a Varian turbo molecular pump (TMP), which is used to achieve base pressures of 1 x 10^{-5} Torr before switching to the ion pumping system. The base pressure achieved with the ion pump after overnight bakeouts was about 1 x 10^{-9} Torr, but repeated thermal desorption experiments led to working pressures of 5 x 10^{-8} Torr.

Since all TPD experiments involve heating and dosing at a distance from the ion pump, pressures must be measured at several points along the vacuum lines using Bayard-Alpert ionization gauges. Figure 2.1 gives the location of these gauges in relation to the sample chambers. Base pressures reflect the measurements taken at gauge three.

The sample chamber consists of a vertically mounted quartz tube sealed at both ends to metal flanges. The top of the tube is closed by another flange holding two copper feed-throughs which are used to connect a thermocouple temperature measurement system to the sample. The quartz tube measures 2" in diameter, 14-18" high, and is capable of withstanding sample temperatures greater than 2000°C under UHV, as the quartz itself never exceeds ~ 250°C

B. Temperature Control and Measurement

Temperature measurements can be taken using two different methods. The first method involves the use of a beaded type-S thermocouple inserted into the graphite sample. The copper feed-through provide external connection to a digital display and a feedback controller. The graphite sample is drilled with two holes into the top and one hole out of the bottom. This design provides a V shaped channel as shown in figure 2.2. The thermocouple may be used to measure temperatures between 20-1700°C with an estimated uncertainty of ± 25°C. Temperatures greater than 1750°C will melt the thermocouple junction, thus limiting its range of use. The second method, useful at temperatures greater than 1700°C, requires the use of a double filament optical pyrometer. The pyrometer is calibrated to measure temperatures between 1100-1900°C with an uncertainty of ± 50°C in reference to the thermocouple. Experiments which require high temperature TPD scans are hung from the copper feed-throughs using a tungsten molybdenum alloy wire as illustrated in figure 2.3. This sample mount requires the removal of the thermocouple device

and thus both methods cannot be use in conjunction except during the pyrometer's calibration between 1100-1650°C.

Temperature control of the graphite sample is achieved via the use of a 400 kHz frequency water cooled induction coil. Simpkins and Mioduszewski have calculated the penetration depth, δ, to be 0.3 cm for isotropic graphite using a 500 kHz rf induction source and similar sample geometry. (8) Penetration depth is defined to be the internal distance that heats to 90% of the external temperature, beyond which the interior of the material is not heated or something like that. Since the frequency of induction is quite similar, we assume that the same δ is also valid for our six turn coil experimental setup. The existence of a penetration depth automatically generates inaccuracies when using optical pyrometry to measure the internal temperatures of the graphite sample. Successful modeling of the temperature gradient can be done, and an external surface temperature of 1800°C corresponds to a temperature at of ~ 750°C. This temperature is taken to be at 60% of the sample radius which reflects the δ of heating inductively. A three dimensional plot of the temperature as a function of both radius and time can be found in figure 2.4

The rate of heating is controlled by changing the power applied to the induction coil. The instantaneous change in power allows for heating rates as slow as 10 degrees per minute to 3000 degrees per minute to be used with simple graphite samples. The higher the sample temperature, the greater the power required to hold and or increase this temperature, which severly contrains the maximum rate of increase. When the intial temperature of the sample is signifcant, 3000°C per minute

rates may not be possible. Samples consisting of metal or metal-carbon mixtures may vary considerably in heating ramp rates and maximum attainable temperature. In general, a 3.4 gram graphite sample can be heated to a maximum of 1850°C, while a 1.5 gram sample can be heated in excess of 2000°C with a six turn coil. Increasing the number of turns on the coil has a direct effect on the efficiency of heating and the maximum attainable temperature.

In addition to the use of an induction coil to heat samples, we may also heat by using an electrical furnace. This system, whose setup is quite similar to those above, relies on a small resistive coil furnace placed around a quartz U-tube. The furnace is controlled by a Love controller and is capable of heating the tube with a maximum ramp rate of 30 °C/min. The maximum attainable temperature using this technique, 1000°C, arises in part from consideration for the structural integrity of the quartz tube under UHV at this temperature.

During heating with an electrical furnace, a type K thermocouple with a feedback loop to the controller is mounted on the outside of the tube in intimate contact with the quartz. Since the heating is radiant rather than inductive, appropriate time must be given to allow each component of the system to reach a stable temperature. Once a reaction temperature is achieved initially, an additional ten minutes is permitted to attain thermal equilibrium.

C. Dosing Gas Introduction

Dose gases are introduced using a separate portion of the vacuum system shown in figure 2.1. The basic setup allows for gases to be fed into 1/4" copper tubing via stainless steel 1/4" tubing which is directly connected to compressed gas regulators. To maximize gas purity, only copper and stainless steel fittings are used to carry gas from the cylinders to the sample chamber. Prior to introducing any gas, a turbo molecular pumped is used to create a vacuum (< 1 mTorr) in the dosing line, this line is then "rinsed" by alternatively pressurizing with the dose gas and then pumping the gas away. This procedure is generally done two times and allows for the removal of unwanted gases which slowly leak into the gas dosing line when left unused. Our tests indicate that these leaks originate from the gas regulators rather than from outside air leaks.

After rinsing, the dose line is pressurized and a portion of this is expanded into the gas introduction chamber. This chamber allows for the final pressure of the gas to be adjusted before it is exposed to the sample. Typically experimental conditions call for 65 mTorr of gas to be exposed to the sample which requires the introduction chamber pressure to be approximately 180 mTorr. Once the sample has reached the proper exposure temperature, the gas is introduced and allowed to react for a predetermined time. Removal of excess dosing gas is done via the TMP, the chamber is switch to the ion pumping system, and sample is allowed to return to room temperature all preceding the TPD scan.

Dosing gases are all of highest purity to maintain well defined reactions. Table 2.1 lists each gas used in dosing and the purity as given by the manufacturer,

Air Products, Inc. The estimation of purity for water vapor has been made based on measurements made with the residual gas analyzer apparatus. Since water is not available commercially as a gas, it must be prepared by removing vapor in equilibrium over a sample of ultra pure water. To purify the water, a small glass bulb containing about twenty milliliters of deionized, doubly distilled water is frozen in liquid nitrogen forcing the gases dissolved at room temperature to become insoluble. This gas is removed from the bulb using the TMP. The ice is allowed to melt and the entire process is repeated at least three times. Dosing with water is then simply done by backfilling the dose line with water vapor in equilibrium above the purified water. The typical pressures used in dosing are slightly higher, about 90 mTorr, since the water vapor is closer to its condensation point and is pumped more slowly.

D. *In Situ* Processing Analysis

The last portion of the experimental apparatus is the use of a residual gas analyzer (RGA) or a quadrapole mass spectrometer (QMS). The detector for the mass spectrometer can be electronically switched between a faraday cup or an electron multiplier to allow for a wide range of scanning speed, resolution, and operational pressure ranges. Pressure measurements using the RGA can range from 10^{-11} or 10^{-12} Torr up to 10^{-4} Torr, depending upon the mass of interest. The RGA provides a digital signal to a IBM compatible computer and can export a spreadsheet containing TPD scanning data. Integration of pressure over time can be used to determine the total gas pumped away in a specific time period.

The RGA can be used in two separate methods of data collection. The first method involves taking a single bar, or "snapshot" scan from 1-300 amu, or any continuous portion thereof with a resolution of 1 amu. (For example, a scan may be completed from 50-95 amu, but not 34, 37, 68-80 amu) The second method, a multiple ion detection (MID) scan, follows up to 18 distinct masses as a function of time. In practice, a bar scan is taken initially to provide a accurate reading of the background gas levels, while during TPD experiments, MID scans are taken. The output of the RGA gives each mass in terms of a pressure in Torr which can be converted to any other unit provided the pumping speed is known at the RGA head.

Calculation of the pumping speed at the RGA head is done by leaking CO at a calibrated rate into the chamber. A specially designed cylinder and attached valve has been purchased from Vacuum Technology in Oak Ridge Tennessee for this purpose. By measuring the pressure of the CO gas with the RGA we have calculated that the pumping speed of the ion pump at the QMS head is 120 L/s. The value reflects only the pumping of CO and varies with each gas as the ability of the ion pump to ionize the gas molecules changes. In general, noble gases have a markedly lower pumping speed while most other gases, such as H_2O, O_2, and CO_2 have pumping speeds similar to that of CO. An excellent review of ion pumping systems and changes in pumping speed over time can be found in P. A. Redhead's book on ultra high vacuum. (9)

Three different types of carbon were used in the TPD experiments. Each carbon was graphitic in nature as characterized by powder X-Ray diffraction (PXRD)

measurements. PXRD samples were prepared by collecting the fine dust resulting from high speed drilling of each sample. The resulting particles were fairly uniform and gave unambiguous diffraction patterns of carbon in its graphitic phase. Each type of carbon is currently used in X-Ray tube products, or being evaluated for future use, therefore much of the structural information regarding these composites is considered proprietary. The materials will only be identified only by the following names, Toyo, felt, and WVN carbons and carbon composites.

An important property of these carbons is the level and nature of impurities that are present during processing. The Toyo and felt composites have been purified by their respective manufactures using a halogen gassification process which will not be discussed here. There is a suspicion that the WVN composite may contain some metallic impurities, based on the observation of metallic plating of the quartz tube at high temperature. An analytical investigation of the residue will be performed later to investigate the nature and perhaps the extent of impurities. The Toyo and felt materials can be assumed to be free of all impurities down to a 10 ppm level.

Table 2.1: Gas purity as reported by the manufacturer.

Gas	*Purity %*
O_2	99.998
CO	99.0
CO_2	99.8
N_2	99.98
H_2O	~ 98*

* Not supplied by Air Products Inc.

Figure 2.1: Experimental design of TPO apparatus.

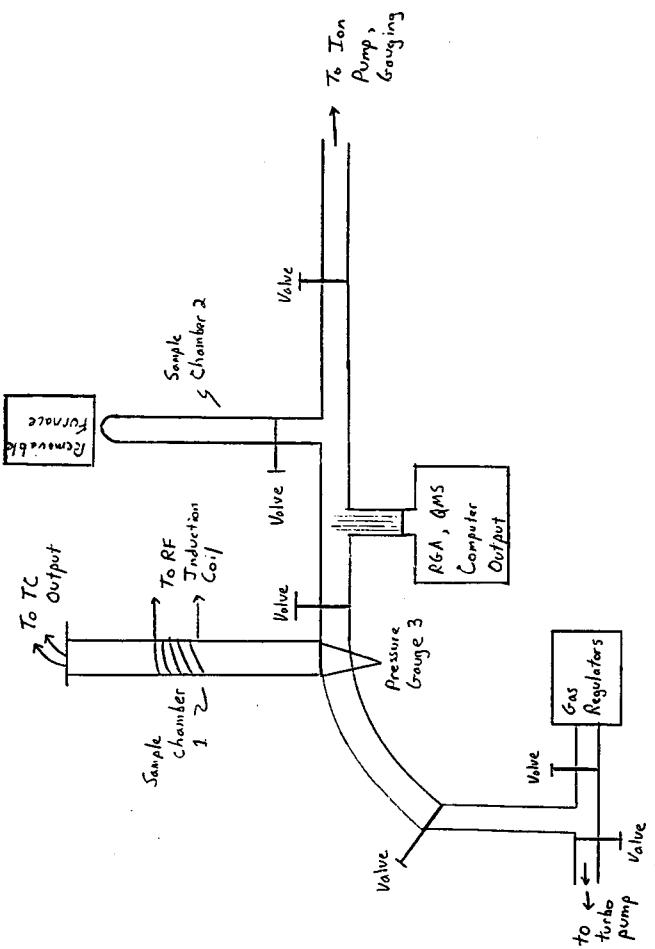

Figure 2.2

Sample design for a Thermo-Couple mount

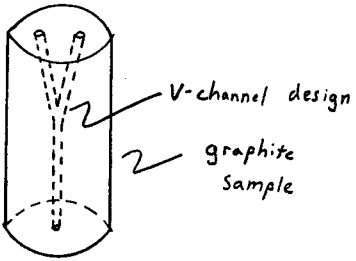

Figure 2.3

Sample design for optical pyrometry mount

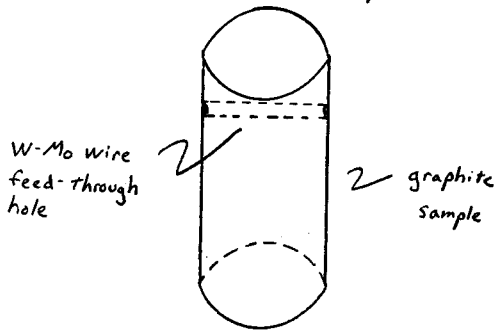

Figure 2.4: Three dimensional plot of temperature, time, and radius for a graphite ingot heated by an induction coil under ultrahigh vacuum. Theory of heat conduction referenced from F.P. Incropera and D.P. DeWitt Introduction to Heat Transfer, John Wiley & Sons: New York, NY, (1996).

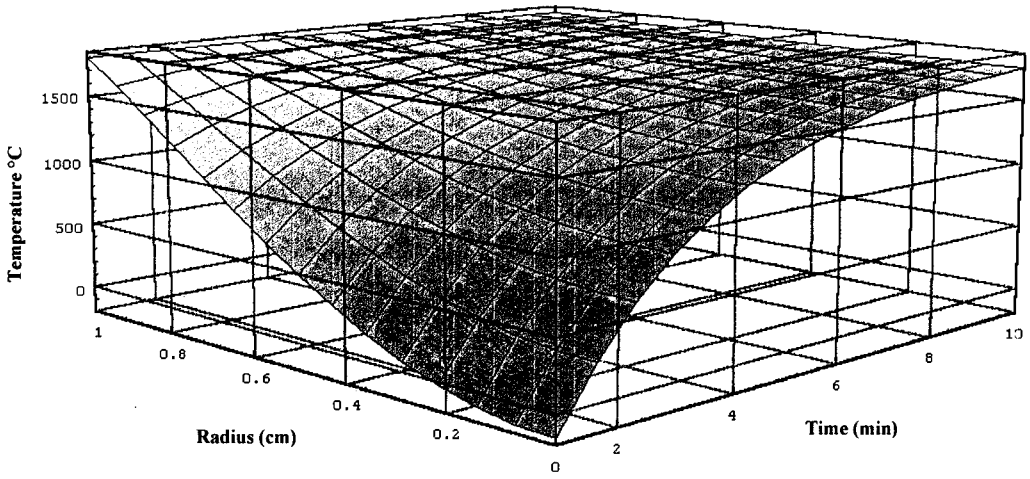

III. Results

The three composite materials show reactivity that is quite clearly similar in some aspects, while being completely different in others. The behavior of each carbon structure will be considered in detail according to the gas used during exposure.

Toyo Graphite Chemisorption. The properties of Toyo graphite have been studied extensively primarily due to its availability from Toyo Tansco of Japan. A sample of Toyo graphite, as-received from the Toyo Tansco Corporation, has a thermal desorption pattern reproduced in figure 3.1. As indicated by the desorption patterns, the surface of the graphite is quite chemically active, releasing significant quantities of H_2O, CO_2, and CO below 1500°C. The second and third TPD scan of this graphite material are shown in figures 3.2 and 3.3. The first TPD scan removed about 99% of all chemisorbed species, resulting in a relatively clean surface. In fact, additional temperature excursions do not significantly alter this TPD pattern any further. The sharp increase in outgassing pressure seen at temperatures greater than 1200°C is the result of another peak between 1200-1600°C which cannot be effectively removed during a lower temperature scan. While desorbing species can be removed during each scan, full removal would require vacuum heating the graphite to 1700°C. In the limits of our experimental conditions, we will therefore assume that the third scan will serve as baseline signal to use as a comparison for the dosing and removal stages.

Oxygen dosing of Toyo graphite proceeds over a very wide range of temperatures as evidenced by the data in table 3.1. Dosing for as little as 23 minutes in the presence of approximately 65 mTorr of O_2 will lead significant desorption of

the CO species during TPD scanning. Figures 3.4-3.8 show the resulting TPD scans after O_2 exposure from 450-650°C in 50°C increments. Dosing appears to be much more favorable at higher temperatures, which we shall see is the result of a high activation energy. (4) By integrating the area under TPD curves, we can measure the relative percentage of surface area covered during exposure. This leads to a good comparison of the type of conditions that enhance the surface reactivity. Figure 3.9 shows how increasing the exposure temperature results in higher surface reactivity.

CO desorption from the graphite is also coupled with smaller amounts of CO_2, C, N, and O desorption as well. H_2O is generally discounted during TPD scans because it is believed that a majority of the water vapor may be from the walls of the quartz tube. An overnight bakeout of the quartz tube and the stainless steel bell jar has been done on occasion before TPD to eliminate this source of water, thus decreasing the extraneous mass 18 signal. With respect to CO_2, since mass 44 desorption after O_2 absorption is generally never more than 10 % of the total CO desorbed, its contribution to the total gas pressure is ignored. The maximum desorption of CO_2 falls between 500-700°C, coinciding with CO desorption. Since a baseline scan reveals very little CO_2 desorption, we assume that any CO_2, like CO, produced is a direct result of reaction with O_2. This observation is entirely consistent with the reaction mechanism proposed by Marchon and workers. (4) At temperatures greater than 1200°C, there is an increase in the pressure of CO_2 which is thought to be related to the CO desorption peak also seen in this higher temperature region.

The mass 28 peak is a combination of the signals from N_2 and CO gas and therefore some further analysis must be done to determine what percentage of the

signal belongs to each peak. Based on well documented fragmentation patterns, if the mass 28 signal was 100% carbon monoxide and had an intensity of 1000 counts/sec, the carbon peak would have an intensity of 7% this, or 70 counts/sec. (10) Similarly, if the 1000 counts/sec was all diatomic nitrogen, the atomic nitrogen peak would be 5 counts/sec. In most of the TPD scans reported, the mass 14 signal is always less than one percent of the mass 28, there are, however, scans when the mass 14 peak is significantly higher. In all cases, a new sample mounted into the quartz tube will exhibit higher than normal desorption of atomic nitrogen during the first TPD run, signifying a mass 28 signal richer in diatomic nitrogen. But in all other cases the mass 28 signal is estimated to be greater than 90% carbon monoxide at temperatures below 1200°C. In light of this fact, we believe that the outgassing of carbon corresponds to removal of carbon monoxide rather than nitrogen containing gases.

Along with the thermodynamic behavior shown in figure 3.9, for which exposure was for twenty minutes at each temperature, there are also kinetic factors governing the chemisorption reaction. A sample exposed for only ten minutes will have a measurably lower percentage of the oxygen chemisorbed species than one exposed for a longer time. This is not to say, however, that several days of exposure will lead to drastic differences in the TPD behavior. As a matter of fact, the kinetic dependence of oxygen chemisorption appears to become insignificant over a period of as little as two days, as a maximum adsorption of O_2 occurs on the surface of the

graphite.[1] That this reaction does not require elevated temperature, is analogous to stating that complete reaction will require a longer exposure time at a lower temperature. Thus in a certain sense, the chemisorption of oxygen, and other gases, will be comparable to a classic kinetics problem reaction described by an activation energy, E_a and a rate constant, k_1 (and consequently will be governed by the same common chemical principles).

Chemisorption of CO follows nearly the same pattern as O_2 exposure, except the relative reactivity towards CO is considerably reduced. Figure 3.10 shows the total outgassing pressure after exposure of the graphite to similar pressures of O_2 and CO. The TPD plots in figure 3.11 show the variation of the mass 28 signal as a function of temperature during desorption. The decrease in reactivity of the Toyo graphite towards CO has also been documented by Marchon and workers, who attribute decreasing reactivity to a higher activation energy of binding relative to O_2. (11) Desorption of CO after CO chemisorption generally occurs between 600-1000°C, which is the same range observed during oxygen chemisorption. The implication is that each reaction involves CO removal from the same precursor species on the surface of the graphite.

As was the case with oxygen chemisorption, the release of CO_2 should be given some minor attention. Figure 3.12 shows the entire TPD scan after CO dosing of Toyo graphite. In this case, the desorption of CO_2 occurs over a broad range between 400-1400°C, as is the case with the atomic oxygen curve. It is interesting to

[1] The maximum adsorption of O_2 does not necessarily signal a saturation condition exists. The total number of active sites on the graphite surface may far outnumber the sites that actually absorb oxygen.

note, however, that figure 3.12 depicts dosing at 65 mTorr, a relatively high pressure for CO; when this pressure is decreased (see figure 3.13), the CO_2 desorption drops to one tenth of the value shown figure 3.12. The C and N curves are at a baseline level, which is expected on the basis of very minimal reactivity with CO onto graphite.

The reactive ability of Toyo graphite dosed with CO_2 is quite comparable to that of reaction with oxygen in the activation energy (E_d) values of desorption. Figure 3.14 shows the TPD scan taken after CO_2 is allowed to react with the Toyo sample for 20 minutes at elevated temperatures. The similarity of this scan with figure 3.8 and 3.12 suggests that the same species in each case serves as precursors to CO removal between 600-1000°C.

There is a slight variation in the CO_2 desorption curve on the same figure. Here the CO_2 curves shifts slightly, desorbing at temperatures between 900-1400°C in one broad feature. The mass 12 curve shows a small peak at 750°C which corresponds to the peak desorption of CO, while the N and O peaks are constant until the TPD scan reaches a temperature greater than 1200°C.

Exposure of the Toyo graphite surface to water vapor at 650°C results in a broad CO outgassing peak which comes off between 700 and 1000°C (see figure 3.15). When the temperature of exposure is decreased to 350°C, CO desorption is quite similar but the range increases to 400-1000°C (see figure 3.16). CO_2, N, C, and O pressures are all very low, the result of carbon's very weak reactivity to H_2O vapor. The temperature range of CO desorption after H_2O exposure suggests that the desorbing species is identical to that released after oxygen, carbon monoxide, and

See page ## for further discussion.

carbon dioxide exposure at elevated temperatures. One mechanism ought to be able to describe all these chemisorption reactions.

As a final discussion of the Toyo graphite surface reactivity, we must consider the high temperature chemisorption reaction observed above 1200°C. Recall from the above discussion that all baseline scans during lower temperature scanning exhibited rising gas pressures as the temperature exceeded 1200°C. Figure 3.17 shows the new baseline scan used for all higher temperature measurements. As was the case with the low temperature TPD experiments, the third TPD scan is used as a baseline. Similar pressures are observed in this plot and will therefore not be reproduced here. Again, as the maximum temperature approaches an upper limit of 1850°C, the pressure of the mass 28 peak begins to rise. Practical limitation of the induction coil and the sample size prevent the temperature from increasing further, but extrapolation suggests another peak at perhaps 1900 or 2000°C. In any event, scanning repeatedly into this temperature region will give us the baseline pressure of CO which is 6 x 10^{-9} Torr.

As we have seen, the exposure of Toyo graphite to O_2 at 650°C leads to the desorption of CO (see figure 3.8). Unfortunately when we attempt to outgas at higher temperatures, we cannot maintain dosing at 650°C while the optical pyrometer is in place. The optical pyrometer is limited to the range of 1040-2300°C and a thermocouple will melt at such high temperatures. Therefore, we chose to increase our dosing temperature to 1040°C. After exposure for only 23 minutes, the TPD scan shows a very broad two-peak CO features from 1200-1600°C (see figure 3.18). These peaks appear each time after exposure and can be removed by raising the temperature to above 1600°C. The C, N, O and CO peaks all exhibit featureless

desorption curves. A slight increase in mass 12 pressure is observed during the most heavy outgassing of CO, but the CO_2 levels are surprisingly small during this higher temperature scan. The bar chart in figure 3.19 shows how the total desorption of Toyo graphite differs above and below 1200°C. The temperature of dosing appears to have no measurable effect on the high temperature outgassing performance. Recent work has compared dosing at 1050°C versus ~500°C with no difference in intensity or desorption temperature being observed.

While several authors have worked with gas desorbed from carbon up to 1200°C, no work has been reported above this temperature. (7) One of the remarkable physical properties of graphite we have found at this temperature is the lack of any annealing processes which would reduce the number of active sites available during adsorption. Repeatability experiments, which take a single sample of Toyo graphite and cycle between dosing and TPD scanning, have total outgassing averages which show less than 15 % relative standard deviation. Even after scanning temperatures approach 2000°C, we are not destroying the active nature of the carbon surface. There is also the possibility that the surface appears as an infinite reservoir of active sites for chemisorption, implying perhaps that active sites are destroyed during the adsorption and removal process but the sheer number of sites would continue to accept oxygen on later scans. We shall consider this possibility later in more detail.

Felt Composite Adsorption. As-received felt composite has a TPD curve as shown in figure 3.20. Similar to Toyo graphite, the surface appears to be responsive during TPD, desorbing simple gaseous molecules after exposure to air at room

temperature. A second scan immediately following the figure 3.20 TPD scan results in the baseline curve shown in figure 3.21. Note that the y-axis has been expanded by a factor of ten. Similar to the Toyo graphite baselines, the curve is nearly featureless until 1200°C where a steady increase in all gas pressures occurs. This increase in gas pressure is thought to be attributed to the same high temperature desorption peak occurring in Toyo graphite between 1200-1600°C. However, we have not verified this suggestion. The CO_2, C, N, and O all show very little fluctuation over the range of temperatures below 1200°C, which is further diminished during the third TPD scan.

The desorption properties of the felt carbon composite after dosing are summarized in table 3.2, which gives CO desorption as a function of dosing temperatures and gas, and the corresponding energies of desorption. A closer consideration of the chemisorption reaction between O_2 and the felt composite reveals that desorption occurs in at least two specific temperature ranges (see figure 3.22). After O_2 exposure at 550°C for 20 minutes, CO desorbs from the surface at 525-875°C corresponding to the same range of E_{des} seen during chemisorption on the Toyo graphite sample. In addition, a second desorption peak is seen between 1000-1275°C whose maximum desorption pressure is double the first desorption peal, which is an entirely separate desorption peak. As with earlier TPD measurements, the pressure of C and CO_2 species correlate with the observed CO desorption patterns. The peak CO_2 desorption occurs at a temperature of 575°C, while the C pressure reaches a maximum between 10 5-1175°C. Both N and O pressures appear to be inactive after O_2 chemisorption. It is not exactly clear why the atomic oxygen curve

remains constant since it should vary with CO and CO_2 desorption. One possible explanation could be that a majority of the atomic oxygen originates from fragmented water, any minor variation due to CO and CO_2 fragmentation could simply be insignificant relative to water's contribution to the signal.

We have ignored any discussion of the peak shapes, but we shall now consider this feature briefly. The lower temperature peak includes a noticeable shoulder to the high temperature side, from about 775 to 975°C. This is in contrast to the peak occurring at higher temperatures which is more clearly defined. A broad peak shape may be the result of several simultaneous reactions occurring at the graphite's surface. Two possible reactions may include rearrangement and readsorption. At higher temperatures, the probability of readsorption may be decreased significantly, which will lead to a smaller range of E_d, or a sharper TPD curve. A reaction mechanism with multiple pathways, such as rearrangements, will lead to a much broader representation of E_d during TPD.

The relative reactivity of the felt composite toward CO at elevated temperatures is less than the reactivity towards O_2 at similar pressures. The Desorption of CO occurs over a broad range from about 600°C to 1200°C and beyond (see figure 3.23). The typical increase in gas pressure beginning at 1200°C limits the amount of useful interpretation that can be extracted from this data. Reaction with CO is not accompanied by the second peak seen after O_2 exposure which suggests that the higher temperature desorption reaction is not possible with CO as the precursor gas. There so little reactivity towards carbon monoxide that very little useful information may be taken from this data and additional experiments must be

conduced in order to map the reactivity further. CO_2, C, N, and O curves are all very flat with little or no response to the small level of CO that is being desorbed. The same general behavior was seen in Toyo graphite when the desorption reaction did not produce significant side products. Attempts to dose the felt material with lower pressures of carbon monoxide gas were unsuccessful, since the reaction simply did not proceed to a significant extent to get reproducible dosing and removal measurements.

Reaction of the felt composite with CO_2 gas yields a TPD scan such as the plot in figure 3.24. The reactivity of the felt towards the CO_2 is doubled compared to the reaction with CO, but still considerably less than the O_2 reacted graphite. The temperature range of CO desorption appears to be divided into two regions, one at 650-1000°C and the other at 1100-1400°C. The outgassing peak corresponding to the higher temperature of desorption is negligible compared to the lower temperature outgassing peak. Perhaps the dissociation of CO_2 into CO and O at these temperatures may contribute to the smaller high temperature peak. Generation of atomic oxygen at the surface of the graphite may lead to species similar to those seen after O_2 exposure (see figure 3.22).

The CO_2 desorption curve is the only other curve that shows some variation from the baseline. The pressure of released CO_2 gas increases at 900°C and slowly continues to climb. Starting at 700°C, the O and C curves also begin to increase in pressure, tracking the increase in CO_2 and CO.

Reaction of felt composite material with water vapor at elevated temperatures leads to a broad desorption of CO at all temperatures above 700°C. While figure

3.25 shows an outgassing signal dotted with maxima and minima, it would be better to characterize this as a broad feature rather than to interpret fine peak structure. We have not previously mentioned very much about the mass 18 signal, but it is interesting to note that it has a maximum that correlates with the CO desorption peak, most clearly seen in this example. Additional experimentation would be necessary to make more specific conclusions regarding this observation. CO_2 desorption follows the same type of slow background increase seen in figures 3.23-3.24, while the C and N peaks remain flat. The O peak is somewhat higher than normal, perhaps a reflection of the dissociation of water molecules at high temperature.

WVN Composite Adsorption. The WVN composite differs physically from the other two carbon based materials since the WVN sample is about 25% larger and about 1 gram heavier than Toyo graphite and about 15% larger than the felt composite. This is not to suggest that each material has a substantial difference in density (although this may be quite likely), rather the physical dimension and therefore overall surface areas may be quite different. This is an important consideration since an increase in surface area will ultimately lead to more surface sites for reactivity. These relative differences must be kept in mind when comparing the un-normalized TPD scan data since the data in this form fail to account for the larger surface area exhibited by the WVN composite materials.

WVN composites shows a surface oxidation reactivity much like the felt and Toyo graphites. Exposure to air for several days leads to a TPD scan similar to that found in figure 3.26. Second and third scans lead to baseline desorption pressures as indicated in figures 3.27 and 3.28. The active desorption of CO at higher

temperatures, readily observed in figure 3.26, is characteristic of the WVN composite material after O_2 exposure. At the same temperatures, CO_2 desorption is absent which is rather surprising based on the magnitude of CO desorption and the small peak in C desorption. This may suggest a significant departure from the standard mechanism of desorption seen in other carbon materials. The second and third desorption scans show very low levels of CO until approximately 1350°C at which point the pressure quickly begins to rise, similar to the behavior of other graphites. Further interpretation of the baseline patterns will not be made here.

WVN composite exposed to oxygen under controlled conditions leads to a desorption pattern such as the TPD scan in figure 3.29. A broad desorption of CO occurs between 525°C and 1075°C, at which point the pressure of CO rises dramatically reaching a maximum near 1225°C and then falling off sharply at a temperature of 1475°C. The desorption occurring in the high temperature region of the scan corresponds to desorption energies on the order of 380-500 kJ/mol, a previously unreported high value. Relatively small amounts of desorption occurs in the conventional lower region from 550-900°C which gives the WVN composite its most significant difference in behavior.

A closer inspection of the minor desorption species during TPD reveals, similar to figure 3.26, CO_2 shows a small peak at 575°C but no peak during the CO desorption at higher temperature. A small broad carbon peak is seen from 1175-1275°C while both the N and O curves show no important features. At temperatures greater than 1350°C, only the CO_2 peak increases while the C, N and O curves maintain a constant level.

Consider the plot shown in figure 3.30 which gives an un-normalized view of composite reactivities. Such a large difference in desorption temperature ranges clearly suggests that different types of active sites are responsible for the high temperature reactivity of the WVN composite, while each composite may share a common type of reactive site. When the mass of each sample is considered, as is the case in figure 3.31, the WVN composite is over three times as reactive as either the Toyo or the felt composite towards O_2. While the macroscopic surface area is larger for the WVN composite, this alone cannot explain the reactivity patterns since the geometrical surface areas are not twice as large.

Exposure of the WVN composite to carbon monoxide at elevated temperatures leads to TPD desorption patterns shown in figure 3.32. The normal mode of CO release occurs over a broad range of 550-1050°C while the high temperature release disappears completely and the surface appears passive in this range. As with the other composites materials, the relative reactivity towards CO is very low; in fact, as figure 3.31 suggests, there is over a ten fold decrease relative to O_2 dosing despite the higher temperature of CO exposure. As suggested earlier in figure 3.9, an increase in the thermal energy supplied during chemisorption should translate to an increased reactivity evidenced during TPD scanning. As expected, none of the other masses show any type of desorption pattern; the signals are identical with the baselines.

WVN composite reaction with CO_2 gas at 650°C leads to a TPD scan as shown in figure 3.33. A broad release of CO occurs between 600-1300°C, accompanied by a slight increase in the desorption of CO_2. Again, the high temperature release of CO seen after O_2 exposure is absent after CO_2 exposure. The

scan is similar to exposure with CO gas and exhibits nearly the same reactivity as well.

Upon heating in the presence of water vapor, a new TPD scan results shown in figure 3.34. CO desorption occurs in two temperature ranges, the first range includes 650-1300°C, while the second range begins at 1400°C and continues above 1600°C. The lower temperature range corresponds to desorption energies between 270-440 kJ/mol similar to Toyo and felt materials, while the higher temperature desorption range represents energies greater than 470 kJ/mol. The WVN shows a very high tendency to react with the water vapor in contrast to the other two materials.

Additional mass signals show very little change from a constant baseline value except for CO_2 curve which continuously increases after 1300°C. Mass curves labeled HC - ## represents masses of expected hydrocarbon fragments which have been found by Marchon et al after water chemisorption. (4) The hydrocarbon fragmentation may be the result of much higher vapor pressures used during dosing as well as physical wetting of the sample's surface by these authors. (4) We do not see any significant signal for these hydrocarbons.

If we suppose that only the top monolayer of carbon is involved in the chemisorption reaction, then increasing the effective surface area of the sample should produce a noticeable increase in the release of CO during TPD. This has indeed been experimentally verified using powdered samples of Toyo graphite, heated using the resistive furnace section of our UHV system. Carbon powder samples are heated initially to 950°C. This first scan, similar to that inductively heated samples, removes all surface oxidation, leaving the material with baseline

desorption properties. If oxygen is exposed to a powdered sample at the same elevated temperatures used during induction heating, chemisorption occurs which can be investigated using the same type of TPD scanning. Figure 3.35 gives the TPD scan on a cylindrical solid Toyo graphite ingot following chemisorption of oxygen via the method of resistive heating. When the same experiment is done on carbon powder with one half the mass of an ingot, the reactivity increases by a factor of eight. Figure 3.36 shows the TPD resulting from chemisorption on the powdered graphite surface. It is apparent that increasing the macroscopic surface area results in a tremendous increase in the number of sites available for reaction. By analogy, an ingot with a rough surface area will appear more reactive than one with a smooth polished surface. This suggests that only near surface sites are accessed during twenty minute doses and room temperature exposures for longer times.

Another important point to make from this experiment are the temperature ranges of desorption agree very well with those taken using inductive heating. CO desorption occurs between 650-900+°C during resistive TPD, while desorption of similarly exposed Toyo using induction heating, desorbs between 550-900°C. These results were obtained using two different type S thermocouples which gives further validity to each method of temperature measurement.

Table 3.1: Desorption of CO after Indicated Gas Chemisorption on Toyo Graphite

Dosing Gas	*Adsorption temp (C)*	*Major Desorption product*	*Maximum desorption temp (C)*	$E_{desorption}$ *(kJ/mol)*	*Assignment*[1]
O_2	450	CO	500-950	210-340	semiquinones
	500	CO	500-900	210-330	semiquinones
	550	CO	550-900	210-330	semiquinones
	600	CO	575-97[illegible]	240-350	semiquinones
	650	CO	575-975	240-350	semiquinones
	1040	CO	1250-1600	430-530	?
CO	550	CO	500-900	210-330	semiquinones
	650	CO	600-1000	240-360	semiquinones
CO_2	350	CO	450-900	200-330	semiquinones
	450	CO	475-900	210-330	semiquinones
	550	CO	575-950	240-340	semiquinones
	650	CO	600-1000	240-360	semiquinones
H_2O	350	CO	400-900	190-330	carbony/semi
	650	CO	700-1100	270-390	?

Table 3.2: Desorption of CO after Indicated Gas Chemisorption on Felt Composite Graphite

Dosing Gas	*Adsorption temp (C)*	*Major Desorption product*	*Maximum desorption temp (C)*	$E_{desorption}$ *(kJ/mol)*	*Assignment*[1]
O_2	450	CO	475-775	210-300	semiquinones
			900-1175	330-410	?
	550	CO	525-875	220-320	semiquinones
			1000-1275	360-440	?
CO	650	CO	700-1000	260-360	semiquinones
CO_2	650	CO	700-1000	270-360	semiquinones
H_2O	650	CO	700-1400*	270-470	?

*** One broad feature**

[1] Marchon, B.; Tysoe, W.T.; Carrazza, J.; Heinemann, H.; Somorjai, G.A. *Journal of Physical Chemistry* **1988**, 92, 5744-5749.

Figure 3.1: As received Toyo graphite, initial TPD scan. Experimental conditions: 20-1550C, ramp rate = 30C/min

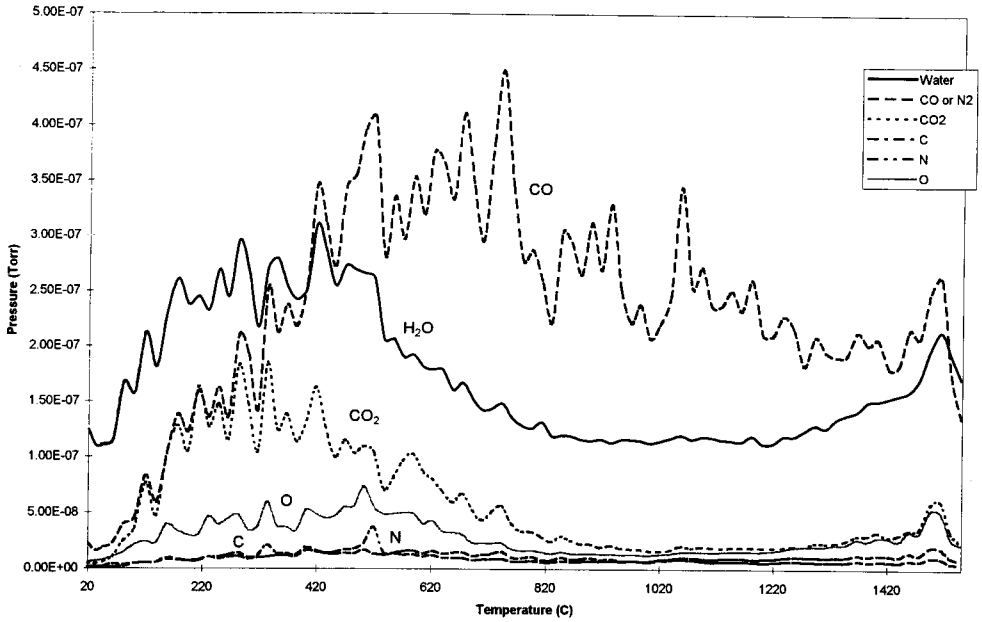

Figure 3.2: Second scan of Toyo graphite immediately following initial TPD run. Experimental conditions: 20-1500C, ramp rate = 30C/min

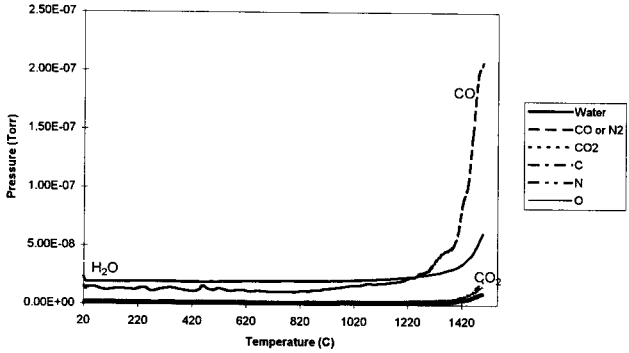

Figure 3.3: Third scan immediately following 2nd TPD scan. Experimental conditions: 20-1500C, ramp rate = 30C/min

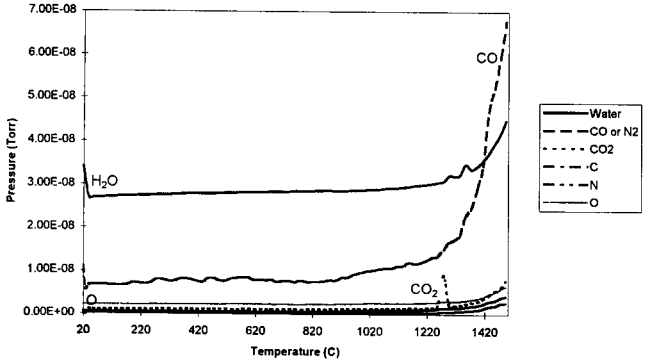

Figure 3.4: Toyo graphite exposed to O2 for 20 minutes at 450C. Experimental conditions: Gas pressure ~ 65 mTorr, ramp rate = 30C/min

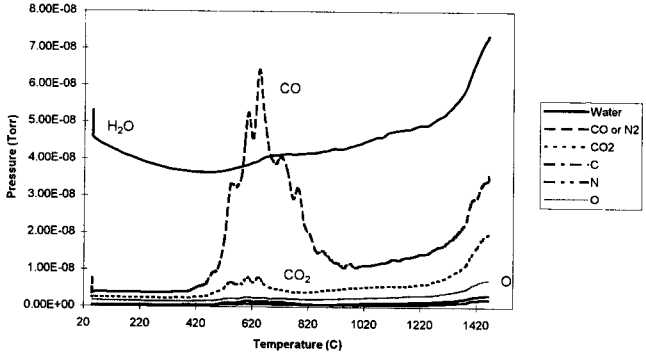

Figure 3.5: Toyo graphite exposed to O2 for 20 minutes at 500C. Experimental conditions: Gas pressure ~ 65 mTorr, ramp rate = 30C/min

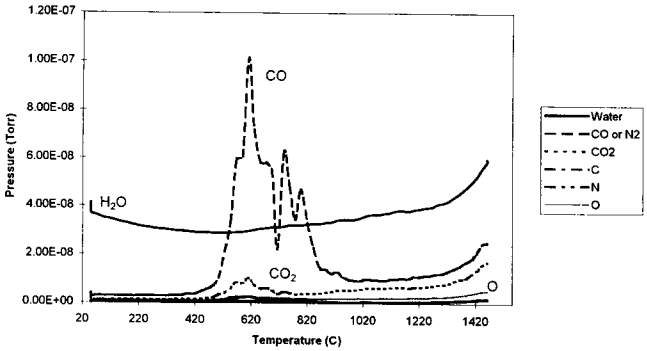

Figure 3.6: Toyo graphite exposed to O2 for 20 minutes at 550C.
Experimental conditions: Gas pressure ~ 65 mTorr, ramp rate = 30C/min

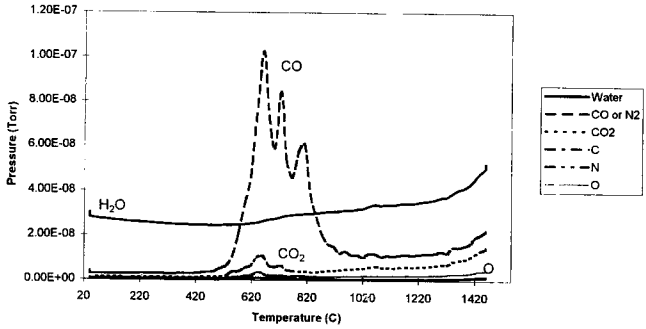

Figure 3.7: Toyo graphite exposed to O2 for 20 minutes at 600C.
Experimental conditions: Gas pressure ~ 65 mTorr, ramp rate = 30C/min

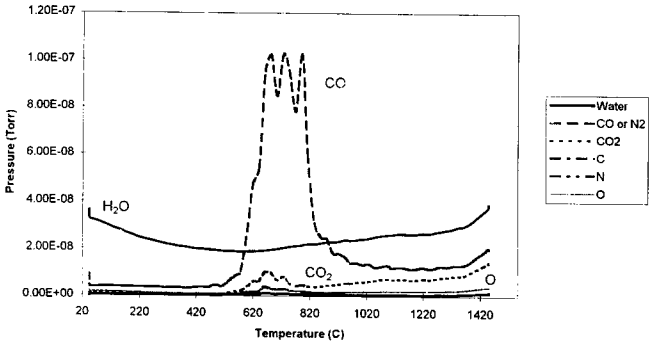

Figure 3.8: Toyo graphite exposed to O2 for 20 minutes at 650C.
Experimental conditions: Gas pressure ~ 65 mTorr, ramp rate = 30C/min

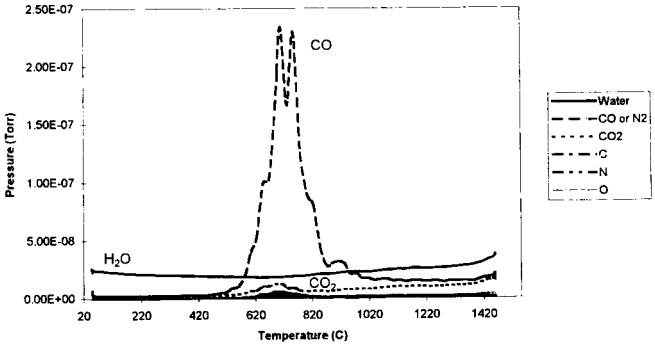

Figure 3.9: Summary of Toyo graphite exposed to temperatures between 450-650C. Experimental conditions: Gas pressure ~ 65 mTorr, ramp rate = 30C/min

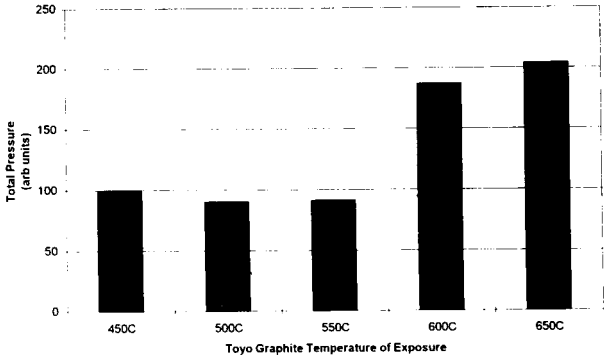

Figure 3.10: Each composite material and the relative reactivity between O2 and CO gas exposure. At elevated temperatures. Experimental conditions: Gas pressure ~ 65 mTorr rate = 30C/min (for Toyo), 50C/min (for Felt & WVN)

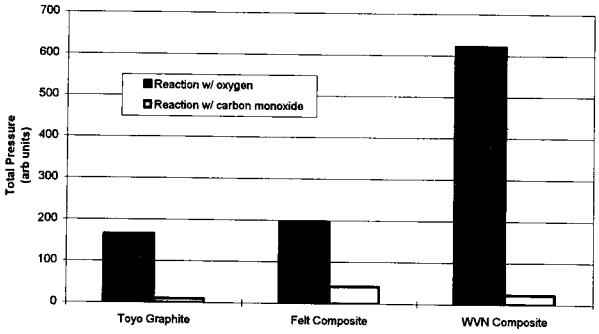

Figure 3.11: Mass 28 desorption following exposure of each composite to carbon monoxide gas. Experimental conditions: Gas pressure ~ 65 mTorr, ramp rate = 30C/min (for Toyo), 50C/min (for Felt & WVN)

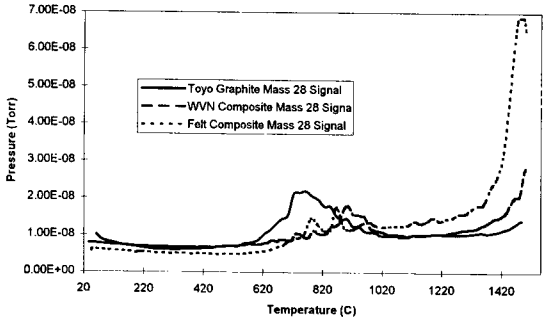

Figure 3.12: Toyo graphite exposed to CO for 20 minutes at 550C.
Experimental conditions: Gas pressure ~ 65 mTorr, ramp rate = 50C/min

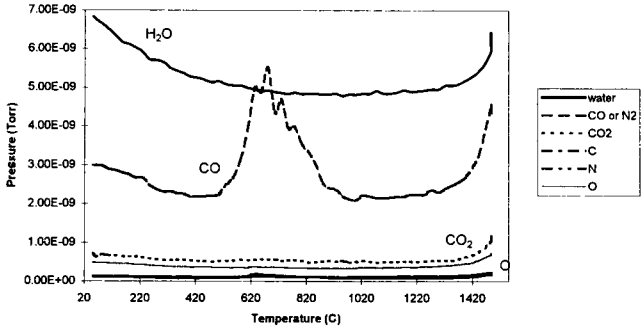

Figure 3.13: Toyo graphite exposed to CO for 20 minutes at 650C.
Experimental conditions: Gas pressure ~ 65 mTorr, ramp rate = 50C/min

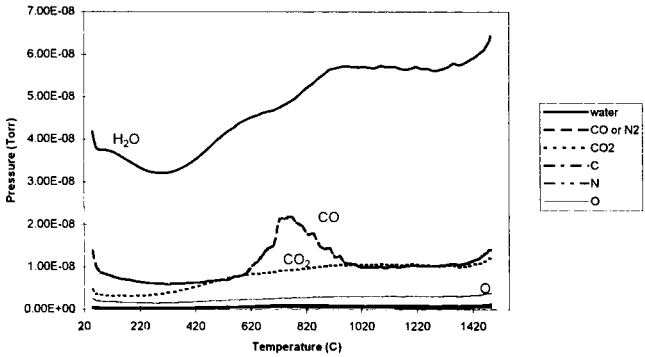

Figure 3.14: Toyo graphite exposed to CO2 for 20 minutes at 650C. Experimental conditions: Gas pressure ~ 65 mTorr, ramp rate = 50C/min

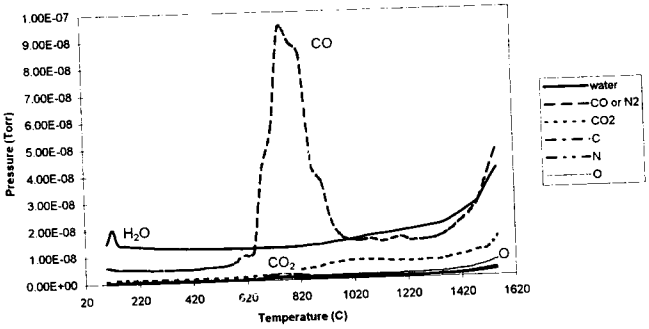

Figure 3.15: Toyo graphite exposed to H2O for 20 minutes at 650C. Experimental conditions: Gas pressure ~ 65 mTorr, ramp rate = 50C/min

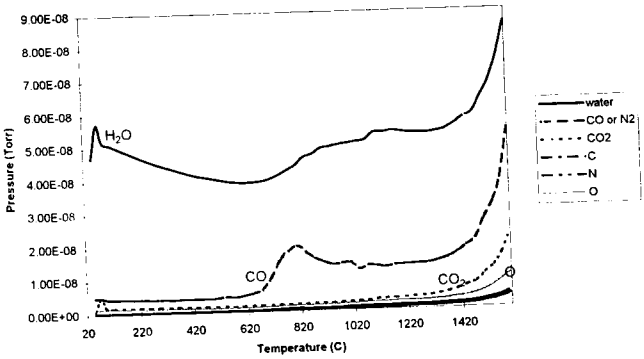

Figure 3.16: Toyo graphite exposed to H2O for 20 minutes at 350C.
Experimental conditions: Gas pressure ~ 65 mTorr, ramp rate = 50C/min

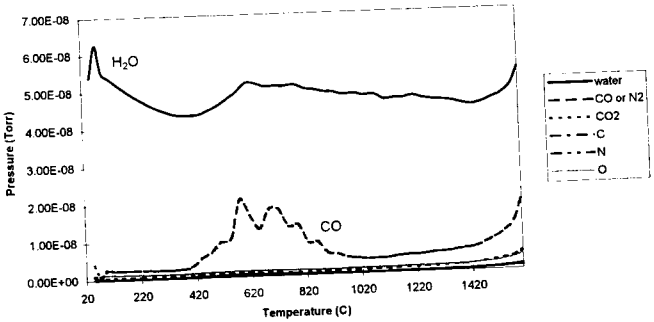

Figure 3.17: Second scan of Toyo graphite immediately following initial high temperature TPD run. Experimental conditions: 1200-1830C, ramp rate = 30C/min

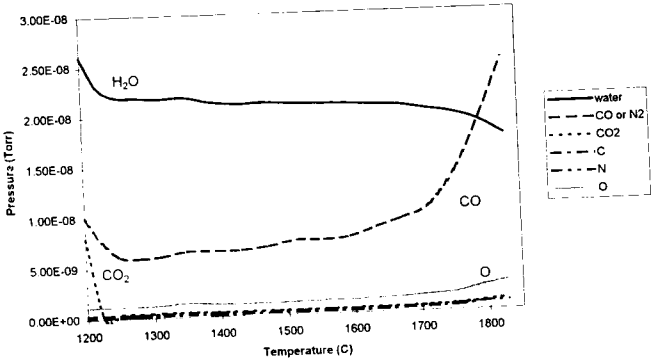

Figure 3.18: Toyo graphite exposed to O2 for 20 minutes at 1040C. Experimental conditions: Gas pressure ~ 65 mTorr, ramp rate = 50C/min

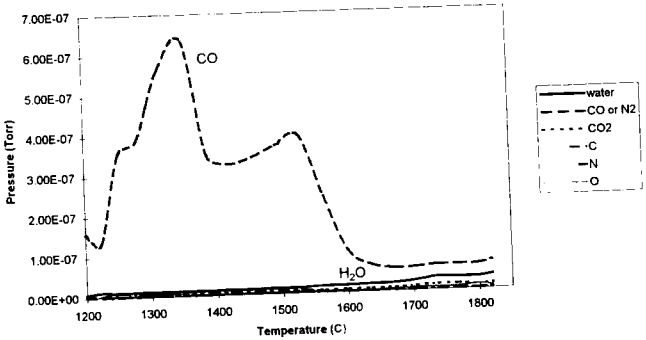

Figure 3.19: Outgassing characteristics of Toyo graphite at temperatures above and below 1200C.[a]

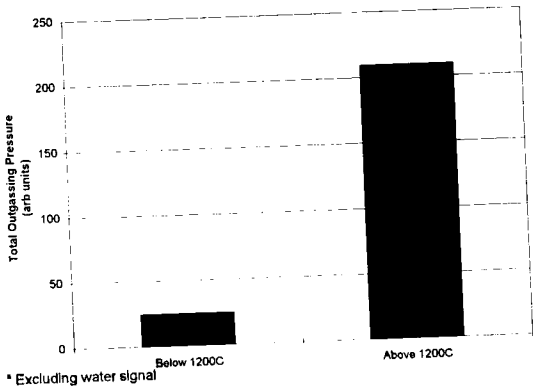

[a] Excluding water signal

Figure 3.20: As received Felt composite graphite, initial TPD scan. Experimental conditions: 20-1640C, ramp rate = 30C/min

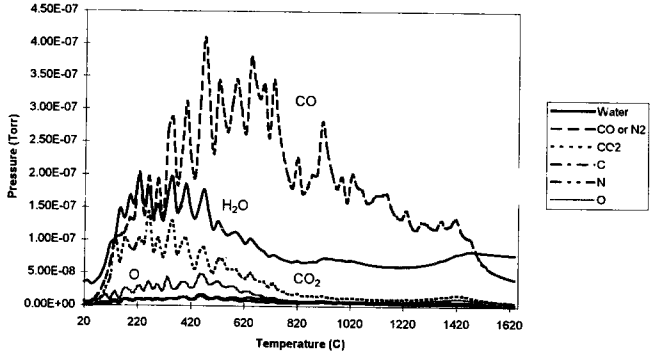

Figure 3.21: Second scan of felt composite graphite immediately following initial TPD run. Experimental conditions: 20-1600C, ramp rate = 30C/min

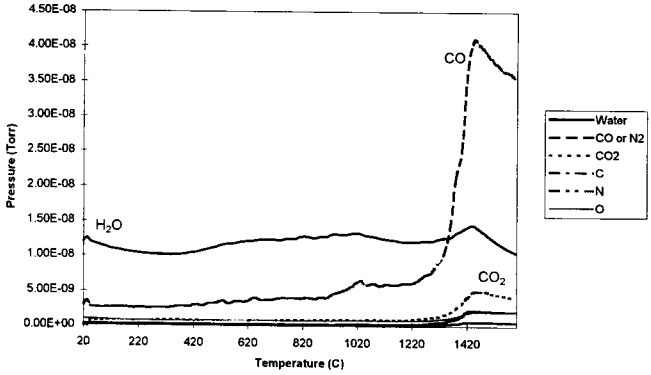

Figure 3.22: Felt composite graphite exposed to O2 for 20 minutes at 550C. Experimental conditions: Gas pressure ~ 65 mTorr, ramp rate = 30C/min

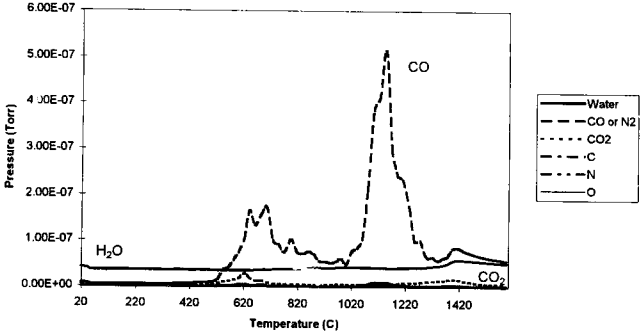

Figure 3.23: Felt composite graphite exposed to CO for 20 minutes at 650C. Experimental conditions: Gas pressure ~ 65 mTorr, ramp rate = 50C/min

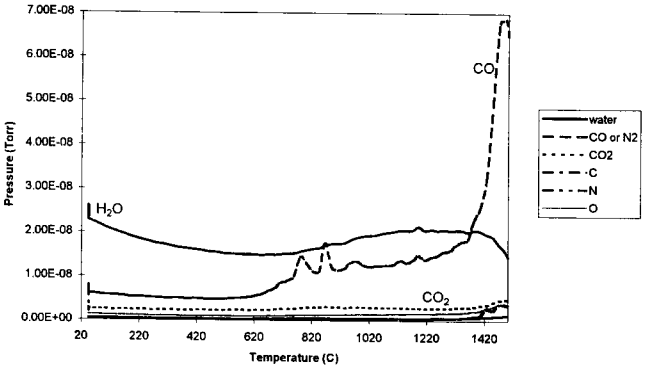

Figure 3.24: Felt composite graphite exposed to CO2 for 20 minutes at 650C. Experimental conditions: Gas pressure ~ 65 mTorr, ramp rate = 50C/min

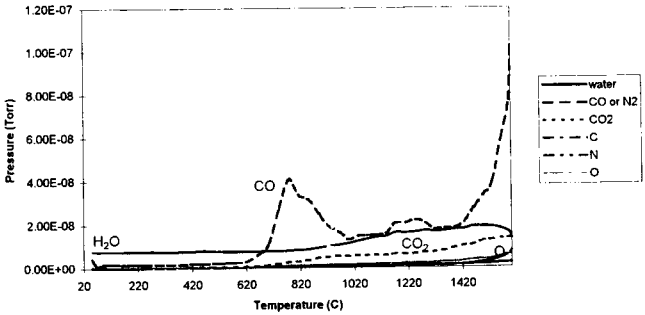

Figure 3.25: Felt composite graphite exposed to H2O for 20 minutes at 650C. Experimental conditions: Gas pressure ~ 65 mTorr, ramp rate = 50C/min

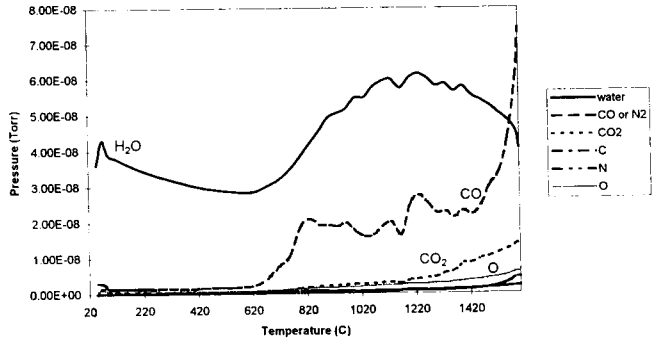

Figure 3.26: As received WVN composite graphite, initial TPD scan. Experimental conditions: 20-1540C, ramp rate = 30C/min

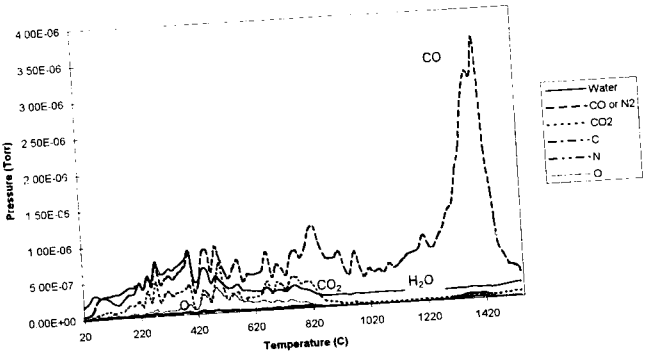

Figure 3.27: Second scan of WVN composite graphite immediately following initial TPD run. Experimental conditions: 20-1600C, ramp rate = 30C/min

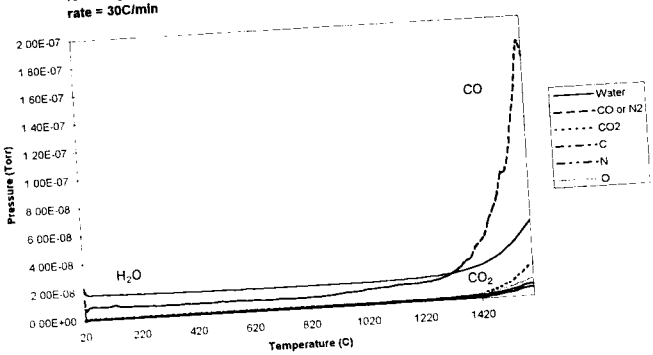

Figure 3.28: Third scan of WVN composite graphite immediately following second TPD run. Experimental conditions: 20-1610C, ramp rate = 30C/min

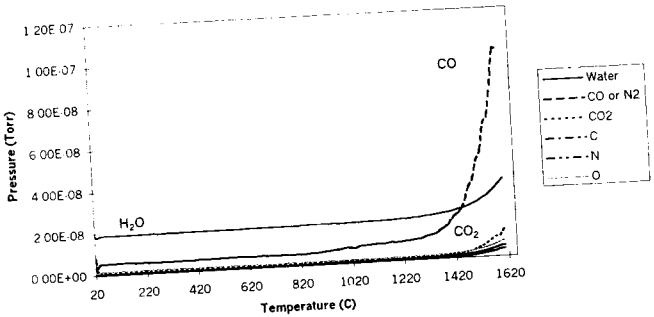

Figure 3.29: WVN composite graphite exposed to O2 for 20 minutes at 550C. Experimental conditions: Gas pressure ~ 65 mTorr, ramp rate = 30C/min

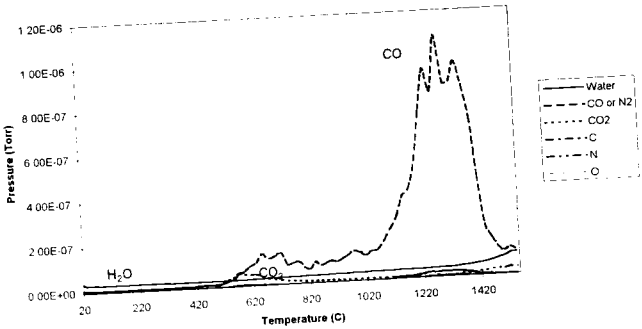

Figure 3.30: Mass 28 desorption following exposure of each composite to oxygen gas. Experimental conditions: Gas pressure ~ 65 mTorr, ramp rate = 30C/min

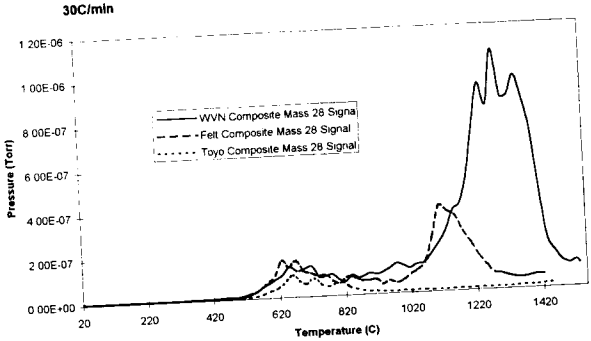

Figure 3.31: Total integrated outgassing intensity for each composite material. Experimental conditions: O2, CO ~ 55 mTorr, time of exposure = 23 minutes, total pressures do not include water vapor

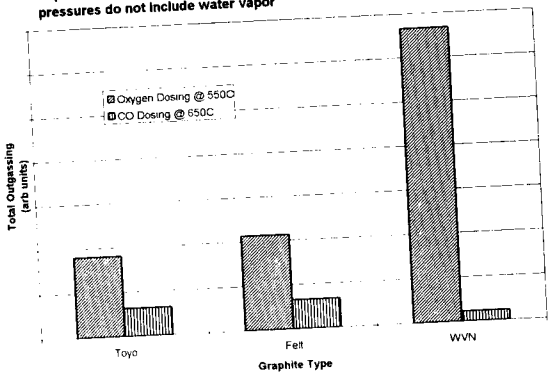

Figure 3.32: WVN composite graphite exposed to CO for 20 minutes at 650C. Experimental conditions: Gas pressure ~ 65 mTorr, ramp rate = 50C/min

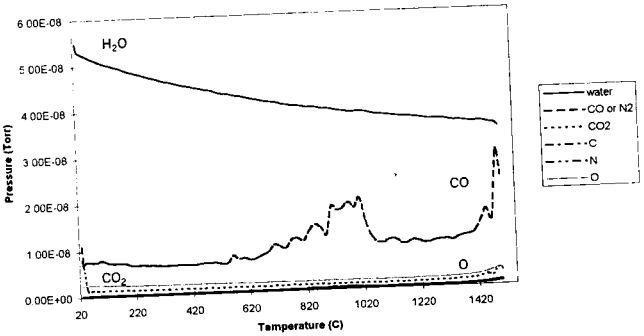

Figure 3.33: WVN composite graphite exposed to CO2 for 20 minutes at 650C. Experimental conditions: Gas pressure ~ 65 mTorr, ramp rate = 50C/min

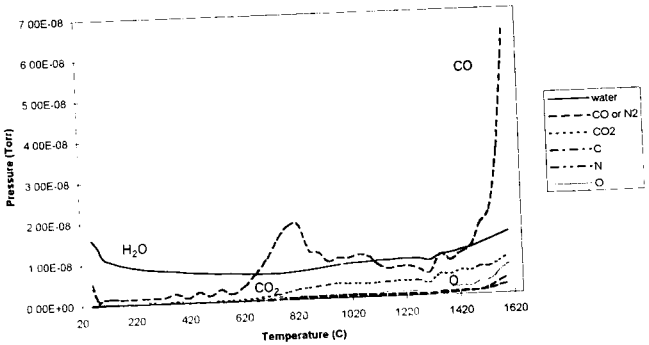

Figure 3.34: WVN composite graphite exposed to H2O for 20 minutes at 650C. Experimental conditions: Gas pressure ~ 90 mTorr, ramp rate = 50C/min

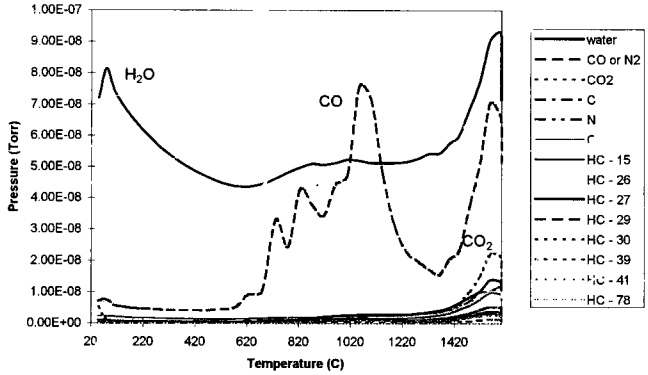

Figure 3.35: Toyo graphite ingot exposed to O2 for 20 minutes at 650C. Experimental conditions: Gas pressure ~ 65 mTorr, resistive heating furnace for temperature variation

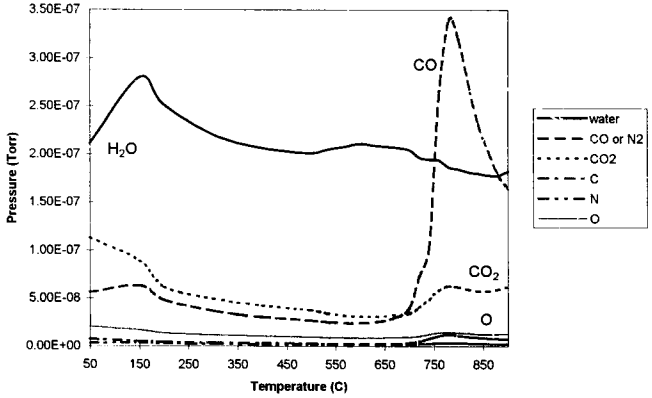

Figure 3.36: Toyo graphite powder exposed to O2 for 20 minutes at 650C. Experimental conditions: Gas pressure ~ 65 mTorr, resistive heating furnace for temperature variation

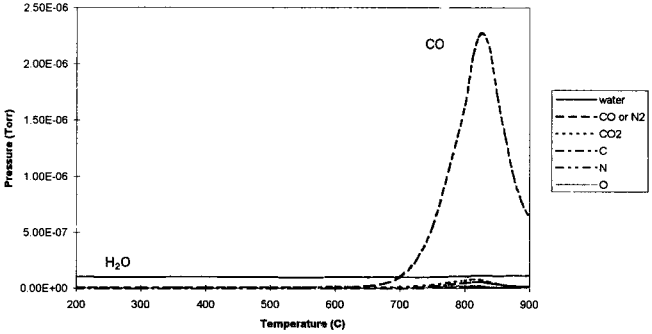

IV. Discussion

The temperature dependence of desorption of species from the surface of the graphite can provide intricate details regarding the chemisorption process which forms those species and the factors that control the efficiency of the reaction. Carbon monoxide removal at several temperature ranges and the availability of atomic oxygen from exposure gas will be discussed using the results of our TPD work. Variation in the reactivity between different composite structures can be catalogued to serve as a basis for further work in this area.

The most recent studies on the gassification of carbon are entirely consistent with the lower temperature findings of our study. (4,7,11) Work done by Marchon et al is summarized in table 4.1 which shows the outgassing of carbon monoxide in response to the exposure of oxygen containing gases. Our experiments have documented surface desorption of carbon monoxide with similar energies as well as similar reactivities. In their experiments, Marchon and workers also reported the reactivity decreased by a factor of ten in response to exposure of carbon monoxide versus oxygen. (11) In a manner similar to what we have found, the outgassing response to carbon dioxide exposure is greater than carbon monoxide exposure, but still less than oxygen dosing. Marchon and workers also found that water dosing produces a desorption signal similar in reactivity to carbon monoxide dosing, with the same range of desorption energies, all reproduced here. Oxygen dosing, which had been reported at temperatures above 230°C, has been found to occur at room temperatures, but with different rates. (4) If room temperature exposure results in the desorption of N moles of gas after a time t_1, then at higher temperatures the exposure

time required to produce the same N moles of gas will be t_2. T_2 will be less than t_1 which is equivalent to saying that dosing can be accelerated by applying the appropriate level of thermal energy. Despite differences in carbon microstructures the results in each study were mutually consistent.

In regards to the high temperature work done by Pan and Yang, we have been able to report desorption data above their 1500°C experimental limit. (7) As was suggested in their findings, strongly bonded surface oxides can be removed at elevated temperatures without an extensive isothermal heating period. In addition, we have supported their conclusion that the amount of gas removed at higher temperatures is a significant portion of the total outgassing. (7) Pan and Yang have also modeled a precursor to carbon monoxide desorption which has been modified slightly in our study to include both the upper and lower planes of graphite which together participate in bonding with atomic oxygen. (7) A revised model will be discussed in much more detail shortly.

Even with the similarities in temperature ranges and desorption energies to the data obtain by Marchon and workers, we are still unable to make absolute comparisons between their material and Toyo graphite in terms of absolute reactivities. The primary reason lies in the probable difference in the number of active sites per material or per sample. Our method of sample preparation, dry cut drilling, leads to a complete loss of information about the surface area as reported by the manufacturer. Drilling causes scars on the graphite surface and unless we compute the surface area using BET N_2 uptake analysis, we cannot estimate the

amount of exposed surface area. A second reason for our inability to compare reactivities stems from the difference in exposure techniques used during our experiments. Using the units of a langmuir (1 x10-6 torros) we may standardize our exposure times and pressures, but our dosing temperatures were not identical to Marchon *et al*'s. (4,11) For these reasons, our relative reactivities are only internally consistent, rather than absolutely comparable with values reported elsewhere.

Previous work has established that relatively few of the active sites participate in each gassification reaction. (11) If in fact this was not the case, and greater than 90 % of the active sites were reacting at the specified temperatures and pressures, we might expect to observe two physical limitations as a result. First we would see a time dependent saturation, after which no additional exposure could increase the level of carbon monoxide outgassed during TPD. This physical limitation manifests itself in the function of the magnitude of desorption versus exposure time. If doubling the exposure time resulted in a factor of two increase in the outgassing signal, a saturation condition would not yet exist on the surface. Alternatively, if doubling the exposure times resulted in only a small increase in the outgassing signal and subsequent increases in the exposure time lead to an asymptotic approach to a constant value, the onset of saturation would be occurring. In fact, our experimental work shows this asymptotic behavior in the outgassing signal in response to increasing exposure time. We can therefore conclude that there must be some surface saturation process ongoing. Secondly there would be the question of regenerating the active sites leading to reproducible dosing and removal. Assuming the mechanism proposed earlier for oxygen dosing on the graphite is correct (see figure 1.2), the surface

changes, forming a five membered ring after carbon monoxide desorption. (11) This gives rise to the question of whether these sites may be annealed out by repeated exposure and degassification, evidenced by diminished reactivity after structural changes on the graphite surface. Additional dosing onto the five membered rings would be prohibited unless the source gas contained carbon, thus leading to an annealed surface state. In fact, complete regeneration of the active sites was observed which partially disproves this model. A modification of this model could consider an infinite number of active sites exposed to the reaction gas. Now only a constant percentage of these sites actually reacts with oxygen during the set exposure time. We could still expect to see a time dependent saturation but there would be a lack of any observed annealing process to reduce the reactivity between experiments. This second model is a likely explanation which has been supported by past work. (11) Support for this model also comes from our experiments involving powdered Toyo graphite. By exposing the fine graphite powder to oxygen, a tremendous increase in reactivity results which is analogous to a much higher saturation level. The process of producing fine particles destroys the macroscopic cavities that are believed to play a role in limiting the ultimate level of saturation in the carbon ingot samples.

At this point, we must consider the effects of slow gas leakage on all of our dosing experiments. Our starting gases are all of high purity and so any additional impurities must come from slow leaks. Since air is over 75% nitrogen we would be looking at a very small percentage of oxygen that could be leaking into the system. In the worst case scenario if we assume that we have air consisting of 20% oxygen leaking in to add a total of 5 mTorr out of 186 mTorr of CO, then the oxygen impurity

we have added is only 1 % of the total CO pressure. It is unlikely that such a small quantity of oxygen is capable of gasifying carbon at the levels we have observed. In practice, determining the extent of gassification of carbon after low pressure exposure posed some experimental difficulties. This has made our simulations of leak-like conditions somewhat suspect. In any case, leaks that eventually do add pressure to the system can generally be traced to the gas cylinder regulators which are simply leaking additional exposure gas into the introduction chamber (see chapter 2), and so their importance is diminished even further.

Extensive work in the literature done with simple gases (CO_2, CO, and H_2O) has lead to numerous observations that the temperature range of CO outgassing is the same regardless of the dosing gas. (4,7,11) The only variation arises from the relative amounts of CO desorption in each case. If we assume that desorption in the same temperature region must correlate to identical precursors, then the mechanism that explains CO loss when O_2 is adsorbed, also must explain CO loss from CO_2 or H_2O adsorption on the surface. Since an extraneous atom, either C or H (in water) is present and does not appear to change the temperature of desorption, only atomic oxygen could be the active species. Therefore, if we investigate the relative ease of breaking the O-X bond, where X is either C or H, we should see a corresponding trend during the outgassing carbon monoxide. A greater concentration (pressure) of oxygen during exposure leads to increased coverage on the surface of the graphite which causes more active sites to become oxidized.[1] During TPD, the increased

[1] In actuality, the increase in surface coverage of oxygen is limited to some extent by other factors. See the previous page for discussion of this point in more detail.

number of reacting active sites will appear as a larger carbon monoxide signal. Using ΔH values of the average bond energies we can estimate the reactivity based on the ease of forming atomic oxygen. (6) The trend from least reactive to most reactive is $CO \sim CO_2(2nd) < H_2O < CO_2(1st) < O_2$ which is exactly the trend suggested by our data. Clearly, the dependence on forming atomic oxygen dictates the extent of CO desorption. This idea could be supported by additional studies with such oxygen-containing gases as NO_2 and SO_2.

We shall now shift our focus to the high temperature desorption observed during TPD scanning with Toyo graphite. The high temperature peak which occurs between 1200-1600°C deserves some special attention here since its existence has been unreported until now. A semiquinone structure is unlikely to be stable at such high temperatures and therefore we must consider alternative a more strongly bound species, such as those found in an intercalation compound. (7) If we consider an oxygen atom intercalated between two planes of graphite that is covalently bonded to a carbon atom on each plane, this may serve as a precursor to the release of CO (see figure 4.1). Since there is electron delocalization above and below the rings of benzene, there may be enough electron density to populate the bonding molecular orbital between oxygen and carbon. In fact, it would not be unreasonable to estimate double bonding between at least one side of the bridge based on the proposed bonding distances. Breaking this bridge would require one C - O, one C = O, and three C = C bonds to be broken offset by the formation of a C ≡ O and three C ≈ C bonds, which is shown in figure 4.2. The new C - C bonds would not be full double bonds because

of the loss of resonance associated with forming five membered rings, but there is still ample delocalization of electrons which could cause the bond to be shorter than the single bond length of 1.53 Å. We shall use a simple average of the strength of the double bond versus the single bond strength or 481 kJ/mol in our calculations here. Using the bond breaking and forming guide above to form CO from this bridge would require an estimated + 415 kJ/mol, which is within a reasonable range for the conditions of our experiments.

The carbon oxygen bridge is one good candidate for the precursor to CO removal. It has also been suggested that grain boundary diffusion could cause the same type of bridging between carbon atoms. (7) For reasons mentioned above, diffusion would be restricted to very shallow depths and not penetrate the bulk. Nonetheless, it would be very difficult to differentiate between grain boundary carbon-oxygen-carbon bridging and bridging between the basal planes of the graphite.

The extent to which diffusion of O_2 into the graphite planes might occur is not very well characterized, but the distance is limited by several physical observations. We do not observe any finite time between outgassing and attainment of a specific temperature. That is to say, if the sample was heated to 1600^{0}C instantaneously, there was no observable delay to the start of outgassing pressure. A noticeable delay would signify diffusion according to Fick's second law, and the possibility that reactivity is not restricted to the top monolayer. (12) Fick's law of diffusion only refers to the microscopic diffusion of materials through grain boundaries and crystal structures. It does not consider diffusion into macroscopic pores that are accessible on the surface of the graphite ingot. Macroscopic diffusion in and out of micrometer

sized pores could occur much faster than diffusion through a structure and may be unobservable in our experiments. The best method of judging the diffusion rate is to examine the peak shapes during TPD. Asymmetrical peaks with a shoulder on the high temperature side would be indicative of a diffusion governed process. Unless this shoulder was prominent, however, it could easily be overlooked and might be taken for a purely symmetrical peak, which does not suggest any diffusion related process. The peaks which result from our TPD experiments are always slightly asymmetric indicating limited diffusion in and out of the macroscopic pores. Such a conclusion can be supported by statistical simulations that predict the probability of a carbon monoxide molecule escaping from a restricted cavity. In addition to peak asymmetry, an isothermal TPD scan can also establish diffusion. An isotherm will yield a rapidly decaying mass signal whose slope will be directly dependent on the distance over which diffusion occurs. Since this isotherm is fit best with a polynomial and not an exponential curve, the diffusion represented here is believed to macroscopic in nature.

As discussed in chapter three, the WVN and felt composite materials exhibit CO desorption similar to Toyo graphite after gas exposure at low temperatures. Studies undertaken on the surface morphology using scanning electron and optical microscopy do not indicate any differences between the carbon based materials and the graphite. Consequently, the same mechanisms are believed to apply in each case which require the formation of atomic oxygen as the initial step and are independent of the initial gas used. Small variances that might be seen in the tables are just due to different dosing temperatures and estimating the temperature on each side of the peak.

This is a minor point and we have assumed that each curve is sufficiently overlapping, within experimental error, to assume they are in fact equivalent. An exception to this rule is H_2O dosing which causes CO to desorb over a broad temperature range for both composites, in contrast to Toyo graphite. The broad desorption band could be due to secondary sources of water vapor readsorbing on the surfac of the carbon and then quickly reacting to form CO. One source of H_2O could be the walls of the quartz tube as they are slowly heated during TPD scanning. Water removed in this manner could then collide with the hot surface of the carbon causing instant decomposition into atomic oxygen. Unreacted water could simply be directly pumped to the mass spectrometer which would explain the broad desorption of mass 18 occurring at the same temperature range as CO desorption.

Another possibility is that there is an impurity in the composite structure that is capable of bonding the water vapor at very high temperatures. If an impurity, such as iron, was on the surface it could react to form surface oxides or hydroxides which could be released as atomic oxygen. Atomic oxygen near the surface could migrate and have a very good chance at readsorption forming CO. This CO would desorb at temperatures corresponding to the iron water bonding rather than the carbon oxygen reaction. The iron-water bond is probably not strong enough to withstand 800°C, but consider instead the ionic Fe-OH or Fe-O bonds which could arise if the metal impurity was in a reduced state. Both the Toyo graphite and the felt composites are believed to be free of most impurities, but ash content test are only available for Toyo graphite.

In addition to H_2O exposure, the WVN and felt composite also exhibit a tremendous difference to O_2 dosing at temperatures greater than 975°C. Neither of the high temperature peaks seen for the felt composite or the WVN composite show up on the Toyo graphite scan, which may reflect a difference in processing of the materials. For the WVN composite material, this is thought to be largely the result of impurities incorporated into the carbon. Heating the WVN composite to 1200°C induces metallization of the quartz tube surrounding the sample, which has not been observed for either the felt composite or Toyo graphite. In general, metals have been shown to bond carbon monoxide quite easily to the surface which may then undergo further dissociation into atomic carbon and oxygen species. (13) Therefore, desorption of carbon monoxide at temperature between 900-1100°C may proceed through a drastically different mechanism involving metal to carbon bonds rather than the previously defined semiquinone structures. While the metal impurities may help explain the behavior of WVN composite to oxygen, this does not help explain how the felt material could also exhibit the same general behavior, different only in the temperature range of desorption.

One last observation to make is that there appears to be a very strict relationship between the energy applied and the molecules that will desorb at that temperature for each composite and graphite material. If a CO molecules requires 450 kJ/ml to activate desorption, it will not release if 350 kJ/mol of energy is supplied for any practical length of time. If the temperature is held constant and the desorption as a function of time is followed, CO outgassing will quickly return to a baseline level

after the first ~ 360 seconds of outgassing. Any additional increase in temperature will cause the CO outgassing level to return to a much higher level, as if no temperature hold had occurred. The implications are that the last temperature the graphite reaches will dictate how free the surface will be from outgassing. For example, suppose during processing that the graphite is heated to 1100°C for 1 hour. If a TPD scan is done on this piece, the surface will look clean until 1100°C is reached, at which point if the temperature is increased, the surface will again appear to be "dirty". Thus, to clean the surface of the graphite and minimize outgassing in a high vacuum environment, one must heat the graphite to the highest possible operating temperature before the chamber is sealed. "Step and ramp temperature programming" cannot substitute for short high temperature holds.

Table 4.1: Summary of previous work on the outgassing of polycrystalline graphite.

Adsorption Gas	*Adsorption Temp (°C)*	*Desorption Product*	*Desorption Temp (°C)*	E_{des} *(kJ/mol)*	*Assignment*[1]
CO_2	room temp	CO	700-980	270-350	Semiquinone
O_2	230-630	CO	700-980	270-350	
H_2O	room temp	CO	700-980	270-350	
CO_2	room temp	CO_2	150	110	Lactones
O_2	230-630	CO_2	190-650	120-250	
H_2O	room temp	CO_2	130-630	88-210	

[1]**Marchon, B.; Carrazza, J; Heinemann, H.; Somorjai, G.A.** ***Carbon*** **1988, 26, 510**

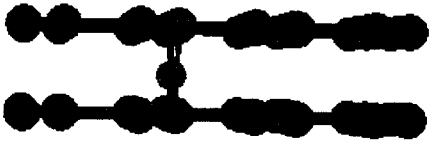

Figure 4.1 (top view): Graphite intercalated with oxygen forming a carbon oxygen carbon bridge. The top side is represented as a double bond, the lower side is a single bond.

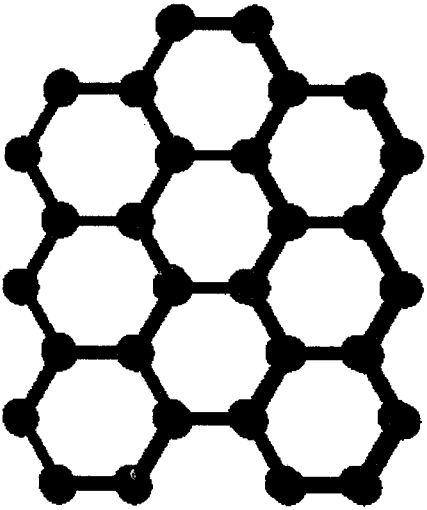

Figure 4.1 (side view)

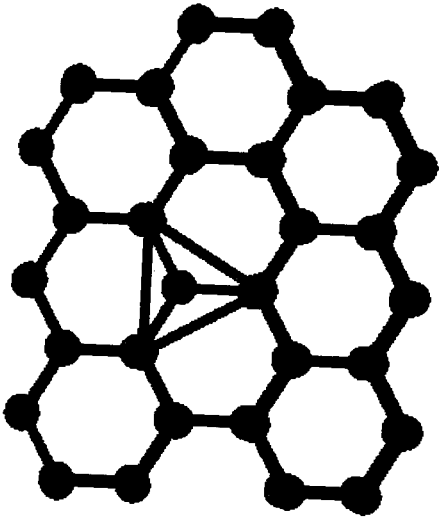

Figure 4.2 (top view): Graphite planes shown after CO desorption. Notice the formation of new five membered rings which complete the structure after CO is removed.

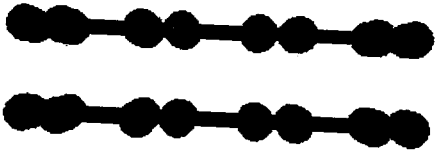

Figure 4.2b (side view)

V. Summary

Oxygen, carbon monoxide, carbon dioxide, and water chemisorb on the surface of graphite and release at higher temperatures as CO gas. The process has been shown to be reversible; repeated removal of CO gas may be accomplished following an exposure step. CO desorption from Toyo graphite occurs between 600-1000°C and between 1200-1600°C. The intensity of the CO desorption peaks have been found to vary with the ease of forming atomic oxygen from the exposure gas. Oxygen has the lowest enthalpy required for forming atomic oxygen and consequently gives the most intense CO desorption signal. Carbon monoxide requires the greatest enthalpy to form atomic oxygen and gives the lowest desorption signal after exposure. The lower temperature desorption peak corresponds to a semiquinone precursor structure, while the higher temperature desorption probably results from an intercalation compound that oxygen forms within the graphite planes. (7,11) Exposure of the composite materials to water and O_2 at elevated temperatures may lead to oxygen metal bonds which could withstand higher temperatures before readsorbing as atomic oxygen and reacting to form CO. We have also been able to conclude that unless the appropriate thermal energy is supplied during cleaning, there is no practical length of time we can heat a graphite sample to remove surface gas. The maximum temperature of operation must be the maximum temperature obtained during cleaning to avoid problems associated with hot high pressure.

VI. Appendices

References

1. M.G. Benz, M.R. Jackson, K.A. Lou, and R.J. Zabala, *Int. J. of Refractory Metals & Hard Materials* **13**, 327-336 (1995).
2. P.L. Walker, Jr., R.L. Taylor, and J.M. Ranish, *Carbon* **29**, 411-421 (1991).
3. R. Schlögl and H. P. Boehm, *Carbon* **21**, 345-358 (1983).
4. B. Marchon, J. Carrazza, H. Heinemann, and G.A. Somorjai, *Carbon* **26**, 507-514 (1988).
5. P.A. Redhead, *Vacuum* **12**, 203-211 (1962).
6. J.B. Umland, *General Chemistry*; West Publishing Company: Minneapolis, MN (1993).
7. Z. Pan and R.T. Yang, *Ind. Eng. Chem. Res.* **31**, 2675-2680 (1992).
8. J.E. Simpkins and P.K. Mioduszewski, *Rev. Sci. Instrum.* **59**, 276-278 (1988).
9. P.A. Redhead, J.P. Hobson, and E.V. Kornelsen, *The Physical Basis of Ultrahigh Vacuum*; American Institute of Physics: New York, NY (1993).
10. A. Cornu and R. Massot, ed., *Compilation of Mass Spectral Data*, Vol 1; Heyden & Sons: London, UK (1979).
11. B. Marchon, W.T. Tysoe, J. Carrazza, H. Heinemann, and G.A. Somorjai, *J. Phys. Chem.* **92**, 5744-5749 (1988).
12. W.D. Callister Jr., *Materials Science and Engineering*, John Wiley & Sons: New York, NY (1994).
13. S. Sung and R. Hoffmann, *J. Am. Chem. Soc.* **107**, 578-584 (1985).